Acoustic Detection of Partial Discharge using Signal Processing and Pattern Recognition Techniques

ACOUSTIC DETECTION OF PARTIAL DISCHARGE USING SIGNAL PROCESSING AND PATTERN RECOGNITION TECHNIQUES

A Thesis in Electrical Engineering

Presented to the faculty of the American University of Sharjah
School of Engineering
In partial fulfillment of
The requirements for the degree

MASTER OF SCIENCE

by

ANAS SWEDAN

B.S. 2007

Sharjah, UAE

May, 2010

ACOUSTIC DETECTION OF PARTIAL DISCHARGE USING SIGNAL PROCESSING AND PATTERN RECOGNITION TECHNIQUES

Anas Swedan, Master of Science

AMERICAN UNIVERSITY OF SHARJAH

ABSTRACT

Power transformers are one of the major components in electric network. The service area of power transformers is quite large which means that the failure of such equipment will cause huge losses for power companies. Therefore, continuous monitoring of power transformers and preventing such failures is of great importance.

During operation, power transformers are affected by different stresses such as electrical, thermal and mechanical stresses. Also, the presence of some defects within the transformer insulation under the applied electrical stress may initiate internal partial discharges. Previous experience has shown that internal partial discharges can cause serious damages for the insulation. Different methods like acoustic, optical and RF sensors were proposed to detect the partial discharge activity. Compared to other techniques, acoustic detection methods are cost effective and less susceptible to noise and interference. In addition, partial discharge (PD) source can be located using multiple acoustic sensors. However, acoustic methods have some drawbacks such as low sensitivity and high attenuation of acoustic signals.

In this thesis, artificial neural networks are utilized to enhance the acoustic PD detection under different insulation conditions. Experimental results have shown that high

detection rates of PD can be obtained under different conditions. Also, classification of insulation condition based on the acquired acoustic PD signals was successful.

TABLE OF CONTENTS

LIST OF FIGURES

LIST OF TABLES

LIST OF ABBREVIATIONS

DFT-Discrete Fourier Transform
DGA- Dissolved Gas Analysis
FFT- Fast Fourier Transform
HF-CT- High Frequency Current Transformer
HPLC- High Performance Liquid Chromatography
HV- High Voltage
MSE- Mean Squared Error
NN- Neural Network
PD- Partial Discharge
PPM- Parts Per Million
PSD- Power Spectral Density
RF- Radio Frequency
RPROP- Resilient Back-Propagation
SDFT- Short duration Fourier Transform
SNR- Signal to Noise Ration
STFT- Short Time Fourier Transform
UV- Ultra-Violet

ACKNOWLEDGEMENTS

I would like to express my sincere gratitude to my advisors, Dr. Ayman El-Hag and Dr. Khaled Assaleh, whose expertise, understanding, and patience, added considerably to this work.

I would also like to appreciate all other people who helped me and supported me.

1. INTRODUCTION

1. 1 Background

1.1.1. General

Power transformers constitute a major part of the electric power network. In fact, the reliability of the power network is mainly dependent on the reliability of power transformers. Also, a large percentage of the capital investment in electric network is allocated for power transformers. Clearly, extending the useful life of power transformers has great economical value [1].

The life span of power transformer is usually determined by the status of its insulation. Therefore, several tests are done in the laboratory to check the healthiness of the transformer's insulation. Such tests include: dielectric dissipation factor test, insulation resistance, hi-pot test and partial discharge measurements. In addition to testing the transformers' insulation during manufacturing, it should be monitored while the transformer is in operation. During operation, the transformer insulation is affected by different stresses which include: electrical, mechanical and thermal stresses. By time, such stresses may alter the dielectric characteristics of the transformer insulation. Also, the presence of some defects within the transformer insulation under the applied electrical stresses may initiate partial discharge activity. Research has shown that partial discharge is one of the major factors that can cause serious damages to the transformer insulation. Hence, on line monitoring of partial discharge signals can be used to evaluate the condition of transformer insulation [2].

The occurrence of partial discharges is associated with different physical phenomena such as: electromagnetic radiation, pressure waves and light. This fact was utilized to develop different techniques to detect the partial discharge signal. Such techniques include: acoustic detection, optical detection and RF antenna. Compared to other detection methods, acoustic emission detection has several attractive points. Acoustic emission detection is relatively a low cost method, it has less susceptibility to noise and electromagnetic interference and it can be used for on-line monitoring of transformer insulation [3]. Also, it is possible to locate the partial discharge activity within the transformer by using multiple acoustic sensors. However, the acoustic technique suffers from some drawbacks such as: the low sensitivity due to the high damping of the acoustic signals because of some

transformer components. Also, the use of multiple sensors for identification of PD location will increase the amount and the complexity of data which mandates the use of some signal processing tools to analyze the acquired data [1].

1.1.2. Definition of Partial Discharge

According to IEC 60270, partial discharge is defined as "an electric discharge that only partially bridges the insulation between conductors". Partial discharge has different measurable quantities such as: apparent charge, repetition rate, average discharge current and quadratic rate [4].

1.1.3. Mechanism of PD generation

The equivalent circuit diagram for a solid insulation material that contains a void is shown in Figure 1.

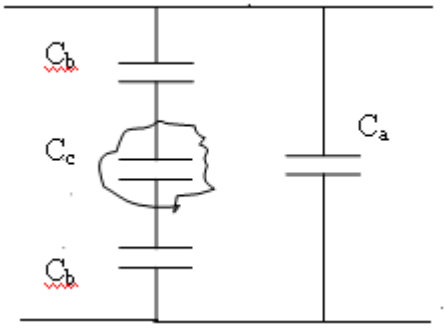

Figure 1: Equivalent cicuit for PD generation

The capacitance value (C_a) represents the healthy part of the insulation material between the high potential and the ground. The capacitance (C_b) represents the insulation that is in series with the cavity. The capacitance of the air void is represented by (C_c). When the applied voltage increases, the electric field across the air void will be enhanced more than the other parts of insulation because of the lower permittivity of air compared to the insulation material. This will continue until the breakdown voltage for the air void is reached, and then voltage across the air void will drop to zero. This will create a potential difference between the two branches and accordingly some charges will move from C_a to C_b. This phenomenon is described as partial discharge.

1.1.4. Types of Partial Discharge

Partial Discharge activity is classified into two main categories; internal discharges and external discharges. Internal partial discharges are usually generated from defects in phase-phase or phase-earth in insulation system that will create high stress at certain

points which will result in small discharges across such defects. Examples for internal partial discharges include: cavity discharge inside transformer winding and treeing channels inside underground cable. The mechanism of cavity discharges was described in the previous section. Another type of internal discharge is treeing channels which usually occur in underground cables as a result of water diffusion.

External Discharges result from the presence of high stress points between the conductors or the conductor and the earth. Examples for external partial discharges include corona discharge and surface discharges. Corona refers to partial discharges in air. It occurs due to electric field enhancement around high voltage equipment. Such discharges may occur around transformer bushings and overhead lines. Another example of external discharge is the Surface discharge. The Surface discharge activity occurs along the surface of the insulation because of the presence of some contamination such as dirt or condensate which will provide a propagation path for the discharge current. This type of discharge may occur in outdoor insulators [5].

1. 2 Detection Methods:

The methods for detecting partial discharge activities are classified into two groups:

1. Electrical methods
2. Non-electrical methods [6][7].

1.2.1. Electrical methods:

Electrical methods include capacitive coupling, CT and RF antenna. Description about each method is shown below.

1.2.1.1. Voltage drop via capacitive coupling

In this method, a coupling capacitor is used. AC voltage is applied across the tested sample as shown in Figure 2. When the partial discharge occurs, the voltage across the sample (represented by capacitance) will drop to a certain value and using the coupling capacitor and the coupling quadripole, the voltage waveform can be measured.

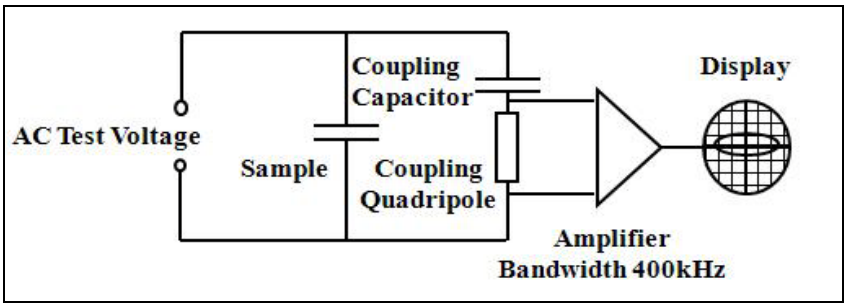

Figure 2: Capacitive detection

1.2.1.2.Induction Detection (Current Impulse)

The inductive detection captures the PD current pulse through the use of high frequency current transformer (HF-CT). When the partial discharge occurs, very narrow electrical current pulses will pass through the grounding conductor. This signal can be detected by using a HF-CT as shown in Figure 3.

Figure 3: PD detection using HF-CT [6]

1.2.1.3.RF Antenna Detection

The RF antenna detection is based on the RF energy generated by the partial discharge. RF antennas can be placed within the power equipment or outside and the RF signals can be acquired and analyzed.

1.2.2. Non-Electrical methods

Non-electrical methods include chemical method, optical, and acoustic emission. Description for each method is shown below.

1.2.2.3.Chemical Detection

Partial Discharge activity results in changes to the chemical composition of the insulation system. Detection of these changes can help to verify the presence of PD activities. There are two major chemical tests for PD detection. The first one is dissolved gas analysis (DGA) and the other is high performance liquid chromatography (HPLC). DGA is used to identify the gas levels in the oil and can be used for both oil and SF6 but it can't be used for solid insulation like cables. HPLC is used to Measure the by-products of transformer wall insulation breakdown.

1.2.2.4.Optical Detection (Light Flash and UV)

The generation of PD activity is associated with a radiation of light in the ultraviolet, visible and infrared ranges. UV detectors were developed to detect the PD activity and to relatively measure its intensity.

1.2.2.5.Acoustic Emission Detection

Each partial discharge activity delivers acoustic energy that can be detected as sound. In practice, there are different types of acoustic sensors utilized in the detection of PD signals. The acoustic sensors have frequency ranges from 0-1MHz. Microphones and piezoelectric transducer are used as sensors. A typical acoustic PD signal is shown in Figure 4:

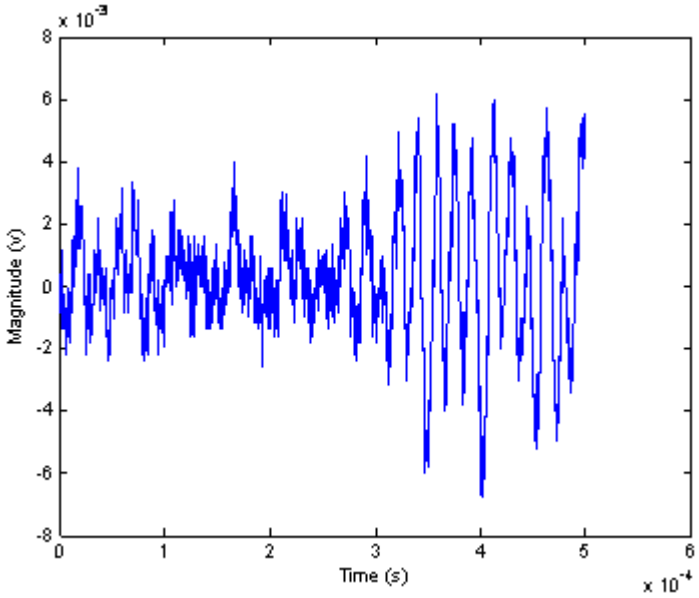

Figure 4: Acoustic PD signal

Table 1 summarizes the advantages and disadvantages for the different methods:

Table 1:Advantages and disadvantages of PD detection methods

Method	Advantages	Disadvantages
Voltage Drop via capacitive coupling	• High accuracy and sensitivity. • Noise immune system.	• Tests are intrusive • Requires external voltage source. • Relatively expensive
Induction Detection (Current Impulse)	• Non intrusive test • No external voltage source is required	• Poor directionality • Low SNR level.
RF Antenna Detection	• Safe method. • Can be used to determine the location of the PD. • Non-intrusive	• Catches RF noise around it. • Needs a line-of-sight • Suffers high attenuation • Expensive equipment.
Chemical Detection	• Inexpensive method. • It is a very accurate method	• Late stage detection of PD • Can't be used for identifying PD source location
Optical Detection (Light Flash and UV)	• On-line testing • Good location accuracy. • Safe method.	• Can detect external PD only • Relatively expensive. • Requires visible line-of-sight • Calibration is not possible
Acoustic Emission Detection	• Less susceptible to noise. • Low cost, small size, portable and accurate method. • Can be used to locate PD • It has a very small false alarm	• Calibration is not possible • Needs acoustic line-of-sight • Provides weak signal so a preamplifier is usually used

1.3. Literature Review

Acoustic emission technique has been utilized for partial discharge detection in different components of the electric network like cables [8] gas insulated substations [9] and power transformers [10]. Moreover, multiple acoustic sensors were used to precisely locate the partial discharge source in power transformers as in [11]. In addition to PD detection and localization, the identification of PD source has great importance. In fact, identifying the source of the PD will help to correctly evaluate the severity of the insulation defect. Several approaches were developed for classifying the different PD sources. In [12] a new approach for the classification of different partial discharge sources was proposed. Partial discharge activity was detected be means of acoustic emission sensor. Eight different types of PD were simulated. The chosen algorithm for training the neural network was the *Resilient Back-propagation* (RPROP). The power spectral density (PSD) and the Short Time Fourier Transform coefficients of the AE were used for training and testing the neural network. It was found that by using STFT, better recognition rates were obtained but the time required for training the neural network was much longer. In this work, the presence of the partial discharge was not confirmed by other PD sensors. Also, optimizing the size of window in case of STFT could be a challenging task because of the variety of PD signals and the difference in the time resolution required for each signal. In addition to using the FFT and the STFT coefficients, wavelet coefficients were also utilized to form the input feature vectors for the neural network as proposed in [13]. The objective of the proposed system was to classify different PD signals based on the PD source. Three different types of partial discharge sources were simulated, namely; sharp-edges, polluted insulators and loose-contacts. The total number of acquired samples was 5100 for each PD type where 66% of the data was used for training the neural network and 34% for testing. The three input components were: the mean of the absolute value, the 2^{nd} and the 3^{rd} order central moments of the wavelet coefficients. The length of the input feature vector was 17 and the hidden layer size was 15 neurons. The recognition rates obtained were in the range of 96-97%. A classification system for different PD sources within high voltage cables was proposed in [14]. Seven different types of defects generating partial discharge within HV cables were simulated in the laboratory. A multi-layer feed-forward neural network was used for the classification

process. Short duration Fourier Transform was performed on the acoustic signal and the SDFT coefficients were used as input to the neural network. For each case, 30 samples were acquired; 10 used for training the neural network and 20 for testing purposes. The recognition rate obtained was 97%. In case of using short-duration Fourier Transform for analyzing the PD signal, the choice of the window size will certainly affect the classification process. Smaller window size provides high resolution in the time domain and poor resolution in the frequency domain and vice versa. This means that some important features might be lost due to the poor choice of window size.

Another important issue related to partial discharges is the evaluation of the transformer insulation based on the acquired partial discharge signal. Although acoustic emission technique has not been utilized to achieve this goal, other sensors were used in insulation assessment. In [15], Current transformer was utilized to detect the partial discharge current. The features extracted from the partial discharge signals were used to classify the aging of the transformer insulation into three different aging periods. The aging periods of the insulation were defined as the insulation-aging period, significant insulation aging and failure imminent. A neural network was used with four statistical features as input. The statistical features used were: skewness, kurtosis, cross-correlation and asymmetry. Particle Swarm Optimization was employed to compute the initial weights and biases of the neural network. A total of 606 data samples were used with 50% of the data for training the neural network and 50% for testing. A classification rate of 96% was achieved in the noise-free case. When noise was added with 30% of the amplitude of original PD signal, the recognition rates dropped significantly to 80%. Other types of features, in addition to the used statistical features, could have been used to enhance the recognition rates. In another work, the partial discharge signal parameters were used to interpret the condition of the transformer oil [16]. Partial discharge was detected using capacitive coupling. The three types of transformer oil used were: clean oil, oil with solid containments and oil with high moisture content. In addition to the different oil conditions, the oil temperature was also varied to account for the different ambient temperatures and the fluctuation in the load. A multi-layer feed-forward neural network with back propagation technique was used for classification. The magnitude of the partial discharge signal and the number of counts were used as input parameters for the neural network. The effect of different parameters such as:

learning rate, number of nodes in the hidden layer and number of hidden layers was investigated. Prediction accuracy with an error of 0.88% was obtained for the classification of the oil condition. In order to better simulate the actual cases, it must be taken into account that the formation of solid containments and high levels of moisture are associated with the aging of transformer, hence the use of aged oil is closer to real cases.

1.4. Proposed research

Partial discharges produce mechanical pressure waves which can be detected using acoustic sensors. However, detection of partial discharge signals using the acoustic emission sensors is affected by different factors such as: the acoustic impedance between the PD source and the sensor and the reflections at the impedance discontinuities. The acoustic impedance of a medium is given by equation 1:

$$Z = \rho V \qquad (1)$$

Where ρ represents the density of the medium and V is the velocity of acoustic signals in that medium [10].

Based on this equation, there is a direct relationship between the acoustic impedance and the density of the medium. The magnitude of the acoustic impedance dictates the amount of attenuation for the propagating acoustic signals. Considering a partial discharge source within the transformer, the resulting acoustic emissions can take different paths until they reach the sensor mounted on the transformer tank. Depending on the propagation paths of the acoustic signals (oil, tank…); different attenuation factors could be encountered. Also the distance between the PD source and the sensor will affect the amount of attenuation. Hence, acoustic PD signals could be highly attenuated which makes the identification of the presence of PD activity using this technique a very difficult task. An example for an acoustic PD signal which was embedded in noise is shown in Figure 5.

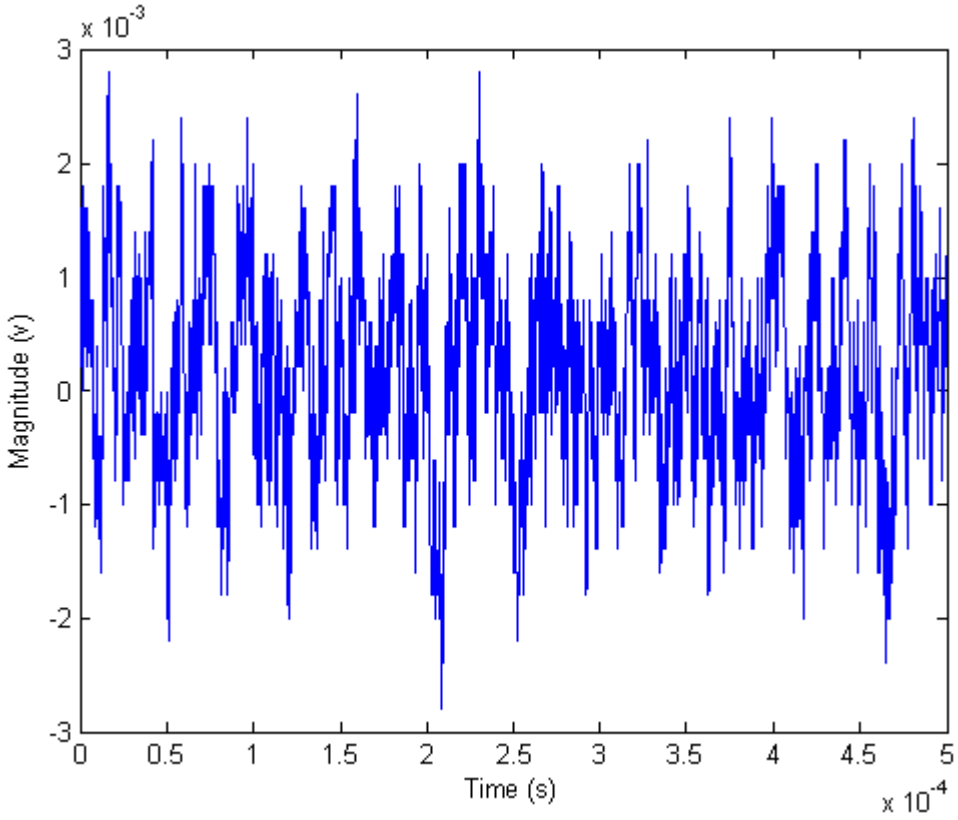

Figure 5 : Highly Attenuated Acoustic PD signal

The acoustic PD signal shown in Figure 5 was highly attenuated due to the long propagation distance between the PD source and the acoustic emission sensor.

The aim of this thesis is to study the possibility of enhancing the acoustic detection of partial discharge signals under different insulation conditions using artificial neural networks. In addition, it aims to investigate the ability to evaluate the transformer insulation condition based on the detected partial discharge signals.

2. MATERIALS AND METHODS

2.1. Experimental Setup

Partial discharge generation and measurements were carried out using the experimental setup in the high voltage laboratory at AUS. The test setup is shown in Figure 6. It consists of a high voltage transformer which was connected to a metallic electrode using high voltage cables. A grounded tank filled with oil was used to model the transformer tank. The digital oscilloscope was utilized to monitor the applied voltage. The generated partial discharge was measured using two sensors; RF antenna and acoustic emission sensor.

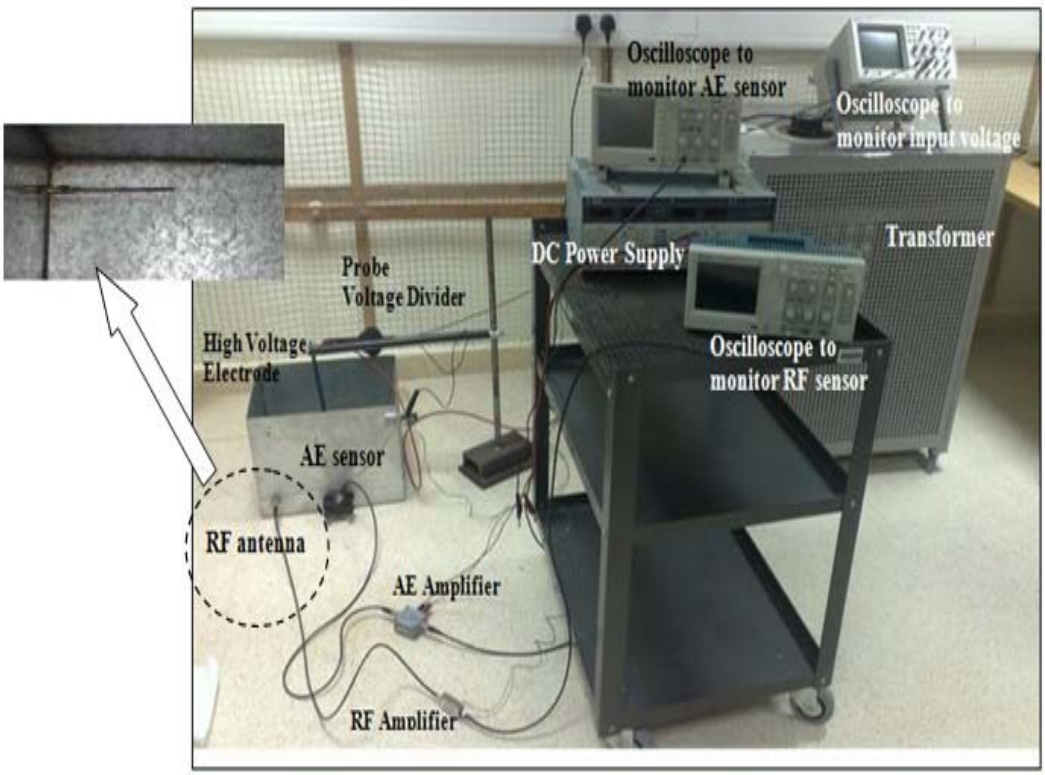

Figure 6: Experimental Lab Setup

2.1.1. Partial Discharge Generation

In order to generate controllable partial discharge signals, a high voltage transformer (AC) with variable output voltage was utilized. The components of the partial discharge generation system are as follows:

a) 15 KVA, 20/22kV Transformer
b) 0-220 V variac

c) Grounded tank: two tanks were used in the PD generation process; tank 1 with dimensions (40×40×40) cm and tank 2 with dimensions of (100×100×50) cm.
d) Sharp edge metallic electrode
e) High voltage probe with ratio of 1/1000.
f) Digital oscilloscope
g) High voltage cables (25 kV)

Oil Samples

Two types of oil were used in the research; old and new oil. The results of the routine oil tests performed for the two oil samples are recorded in table 2:

Table 2: Routine test results for the two oil samples

Tests	Methods	Old Oil Results	New Oil Results
Breakdown voltage (kV)	IEC 60156	27.7	44.9
Water content (PPM)	ASTM D 4928-00	30	12

2.1.2. Partial Discharge Measurements

2.1.2.1. Acoustic Emission Sensor

The acoustic emission sensor was used to detect PD signals created in the air and in the oil. In previous work, it was found that most of the acoustic PD signal energy is in the frequency range 23-80 KHz [10]. Based on that an acoustic sensor with frequency range 20-80 KHz was utilized in the measurements of PD signal. The magnitude of the acoustic signals is low which required the use of a pre amplifier and a band-pass filter to remove the noise from the acquired signal. The characteristics of the AE sensor are shown in table 3:

Table 3: AE sensor

No.	Characteristic	Value
1	Preamplifier gain	46 dB into 50 Ohm
2	Bandwidth (-3 dB)	20-80 kHz (10 Vpp)
4	Power Supply	28 Vdc, 24 mA (no signal), 64 mA,(max. signal),
5	Output connector	BNC
6	Output range	10 Vpp into 50 Ohm

2.1.2.2. Couplant

In order to make the contact region between the acoustic sensor and the tank smoother, silicone greases was used. This has the effect of increasing the quality of the transferred acoustic signals and it will reduce the reflections on the surface of contact.

2.1.2.3. RF antenna:

The aim of using an RF antenna is to ensure the presence of the partial discharge activity. A pre-amplifier was used which operates in the frequency range of 0.5-2 GHz. A typical RF PD signal is shown in Figure 7.

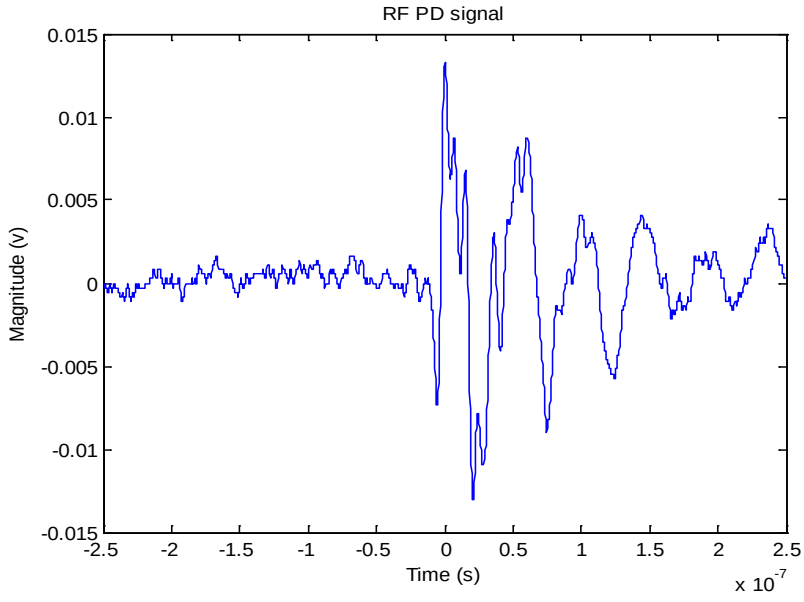

Figure 7: RF PD signal

The detected RF PD signal was used to trigger the detection of the acoustic PD signal as shown in Figure 8.

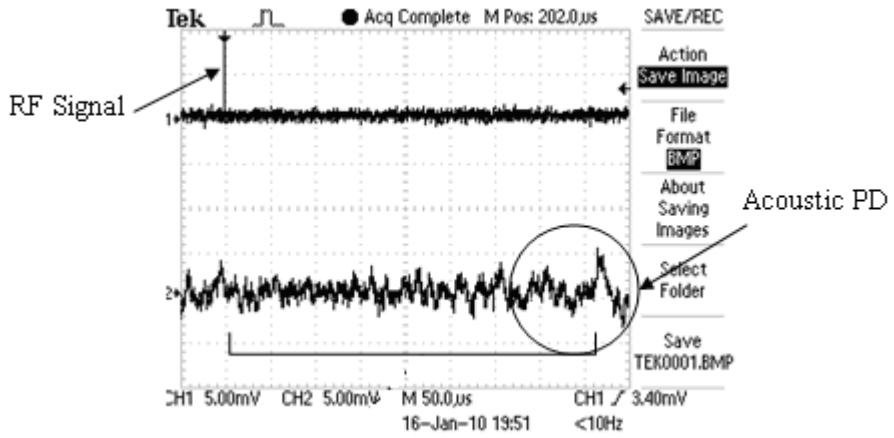

Figure 8: RF and AE partial discharge signals

2.1.2.4. Digital Oscilloscope:

TDS2014B digital oscilloscope is a two channel 60MHz bandwidth with a 1Gs/second sampling rate. It has 8-bit resolution with 2mV/division vertical sensitivity. TDS2014B is not only a data acquisition and measurement device but it has data storage capability with a USB interface. The time resolution was set to be 50µs. When the magnitude of the acquired RF signal (Channel 1) exceeds the trigger level, set at 3.4 mV, the signal from channel 2 which represents the acoustic emission signal is displayed on the oscilloscope and then it can be saved on USB device in excel format which can be transferred to Matlab.

2.1.2.5. Measurements

The measurements of the acoustic PD signal were carried out under different insulation conditions such as new and old oil. In addition, some factors that could affect the propagation of the acoustic PD signals were considered such as: the presence of some barrier (core material, paper insulation), the location of the PD source relative to the sensor and the tank size. Table 4 summarizes the different cases of measurements:

Table 4: Measurments

Case of measurement	Picture
PD source at position a	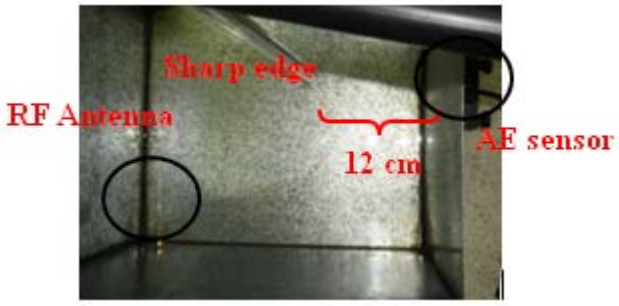
Metallic barrier (core material) inserted between the PD source and the acoustic sensor	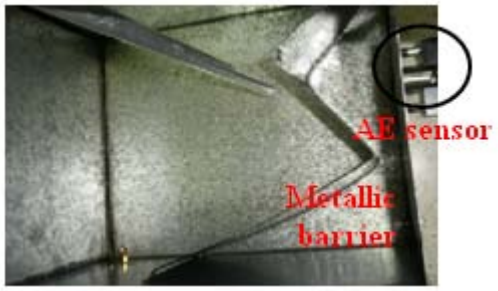
Paper insulation inserted between the PD source and the acoustic sensor	
PD source at position b	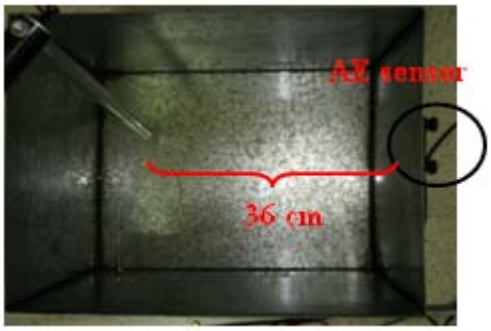

2.2. Classification System:

2.2.1. Pre-processing: Digital filtering:

Before extracting the features for the detection and classification process, the acquired signals were filtered using a digital band-pass Butterworth filter with cut-off frequencies at 25 kHz and 75 kHz. Filtering is required to remove noise and interference outside the range of the sensor. The frequency response of the designed filter is shown in Figure 9.

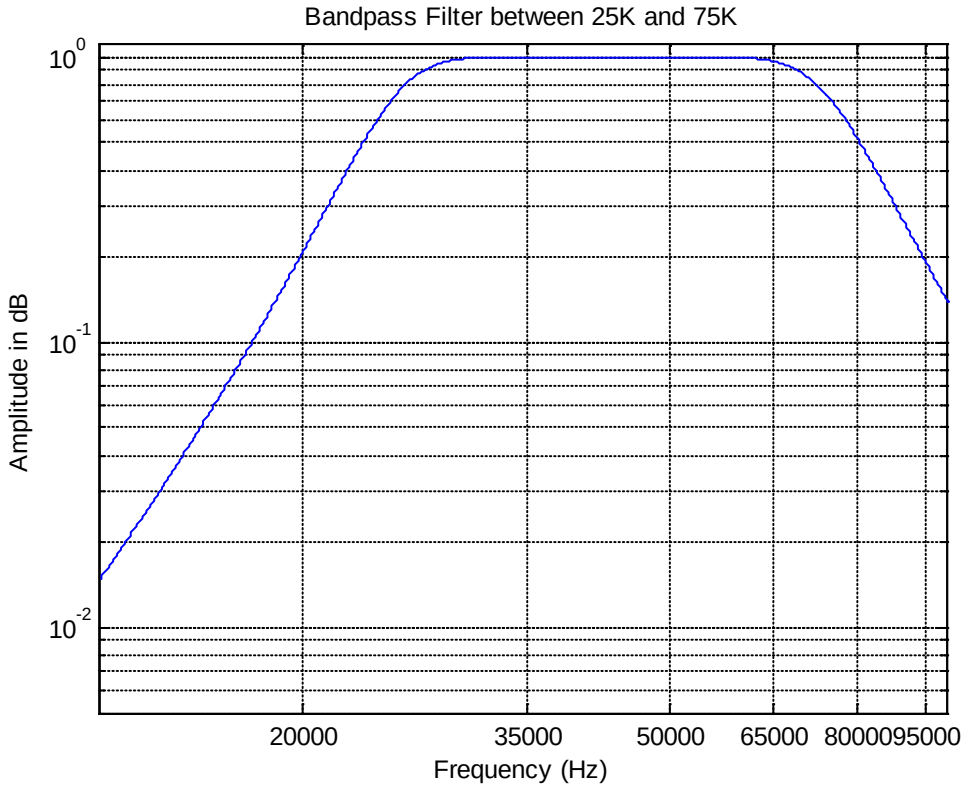

Figure 9: Frequency response of digital filter

2.2.2. Features extraction

Due to the large amount of input data, it will not be possible to process the acquired acoustic signals. Thus, certain features will be extracted from the acquired signals.

2.2.2.1.Wavelet Transform

In discrete wavelet transforms, the acquired signal can be analyzed in two dimensions: time and scale. The scale domain is related to the effective frequency of the mother wavelet. The signal is passed through series of low-pass and high-pass

filters. The output of the high-pass filter is the 'details' which represent the high frequency content of the signal in a certain band while the output of the low-pass filter is the 'approximations' which represent the low frequency content of that band. The methodology of the discrete wavelet decomposition is shown in Figure 10.

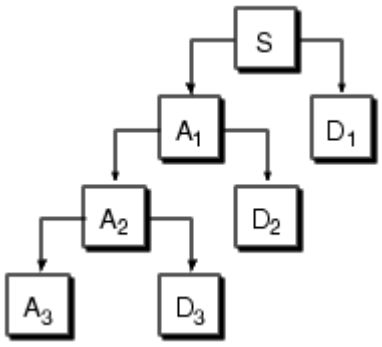

Figure 10: Wavelet methodology

By applying wavelet transform decomposition, the acoustic emission PD signals are decomposed into several details and approximations at different levels. The mother wavelet function used was 'db 15' with 5 levels of decomposition.

Wavelet based features:

1. Entropy

Wavelet entropy is a statistical measure of the energy dispersion among different spectral bands. Basically it describes the "concentration" of coefficients in a certain band. So, wavelet entropy would be large when all coefficients are roughly of the same size and small when all but few coefficients are negligible [17][18]. Entropy of a signal x_i ; $1 \le i \le N$ is given by equation 2:

$$E = -\sum x_i^2 * \log(x_i^2) \qquad (2)$$

2. Variance

The variance of a discrete signal x_i, where $1 \le i \le N$ is defined as shown in equation 3:

$$Variance: \sigma^2 = \frac{\sum_{i=1}^{N} (x_i - \mu)^2}{N-1} \qquad (3)$$

Where μ is the mean value.

2.2.2.2.Kurtosis

Kurtosis is a measure of sharpness for any data distribution with respect to the normal distribution. A normal distribution has a kurtosis of three and excess kurtosis of zero. This is shown in Figure 11.

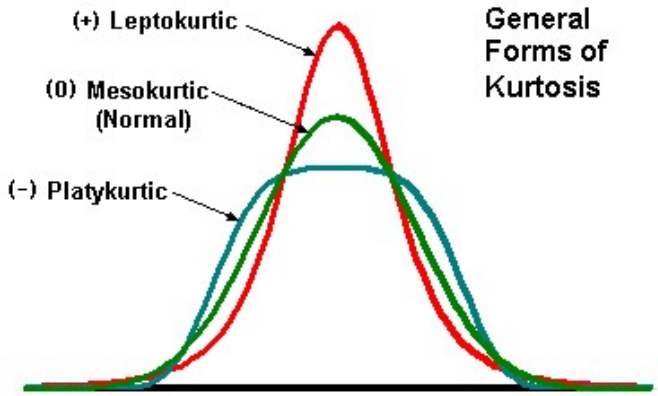

Figure 11: Kurtosis types [19]

The kurtosis of a discrete signal y_i, where $y_i = f(x_i);\ 1 \le i \le N$ is defined as shown in equation 4:

$$Kurtosis: K_u = \frac{\sum_{i=1}^{N}(x_i - \mu)^4}{N\sigma^4} \qquad (4)$$

Where μ is the mean value and σ is the standard deviation.

2.2.2.3.Skewnees

Skewness measures the asymmetry of the data distribution with respect to the normal distribution. If the distribution is symmetric, the value of skewness is zero. If the distribution is skewed to the left or to the right, then the skewness value will be larger or less than zero as illustrated in Figure 12.

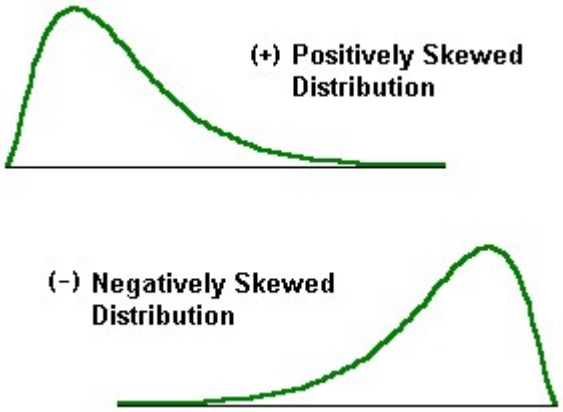

Figure 12: Skewness Measure [19]

The value of skewness measure of the signal y_i, where $y_i = f(x_i);\ 1 \le i \le N$ is defined as shown in equation 5:

$$Skewness: S_k = \frac{\sum_{i=1}^{N} (x_i - \mu)^3}{N\sigma^3} \qquad (5)$$

The extracted features must be processed using a classifier in order to make a decision about the class of the acquired signal. Artificial neural network was adopted as a classifier.

2.2.3. Artificial Neural Network

Due to the complexity of the classification problem, artificial neural network was adopted. A feed-forward neural network with back propagation learning algorithm was used. The architecture of the neural network is shown Figure 13:

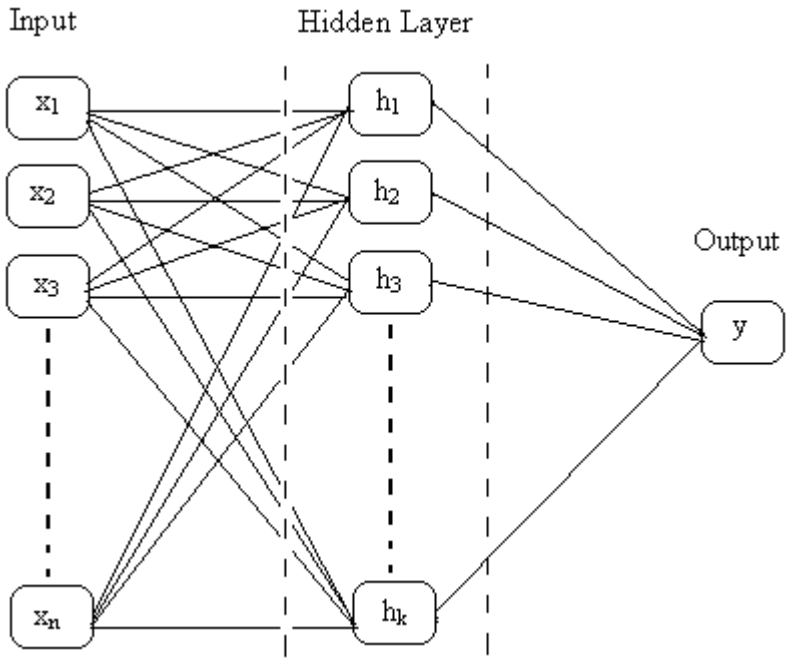

Figure 13: Architecture of NN

The number of hidden nodes was set initially to be twice the number of input nodes, it was then increased until the point where there was no further improvement in the performance of the network. The criterion for measuring the performance of the network in training was the Mean Squared Error (MSE) which reflects the norm of the difference between the output of the network during the training stage and the desired targets. The number of epochs was varied between 1000-2000 epochs. An example of the convergence of the neural network during the training stage is shown in Figure 14:

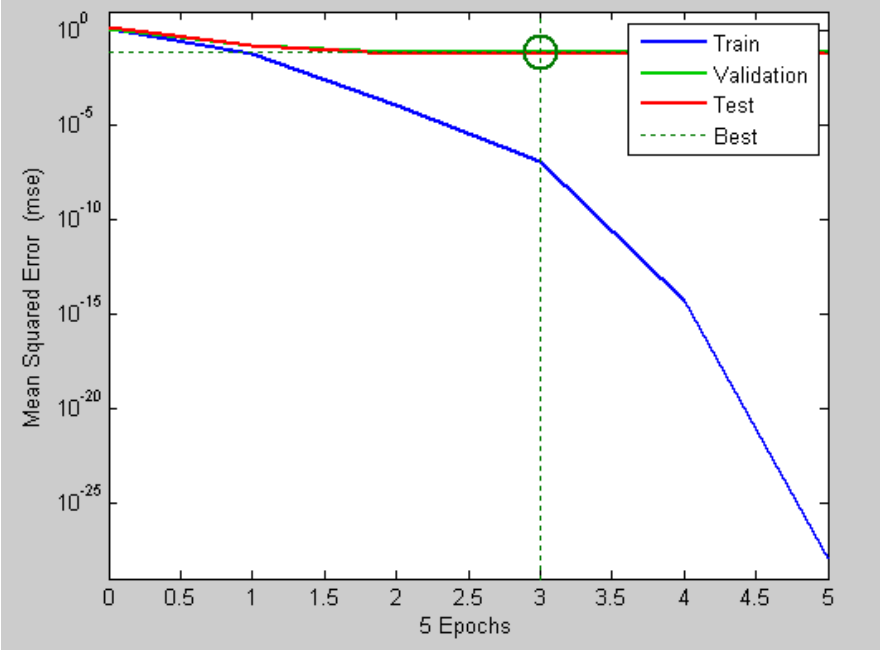

Figure 14: Convergence of NN

The performance of the classification system was evaluated based on the recognition rate which represents the average of the correctly identified signals to the total number of tested signals. False alarms rate was calculated by dividing the number of no PD signals which were incorrectly classified as PD signals by the total number of tested signals. False positives rate was computed by finding the percentage of PD signals which were incorrectly classified as no PD signals.

For each case of measurements, the number of acquired signals was 60 where 80% of the acquired signals are used for training the neural network and 20% for testing. In order to improve the statistical significance of the testing results, the acquired acoustic signals were mixed in 12 different combinations for training and testing the neural network for each case.

Four different types of features were used as the input to the neural network as follows:

1. Kurtosis, skewness values for the acquired signals
2. Variance of wavelet sub-bands
3. Entropy of wavelet sub-bands
4. Discrete Fourier Transform coefficients (DFT) in the range (25-75 kHz). The total number of DFT coefficients in the relevant frequency range is 23 coefficients.

3. RESULTS AND DISCUSSION

3.1. Presence of Partial Discharge Activity

The aim of this part is to verify the presence of the partial discharge activity within the transformer model. Different experiments were designed to simulate actual cases where acoustic emission due to partial discharge activity may propagate through metallic barriers (as transformer core), paper insulation of the transformer windings or through transformer oil. Also, the location of the partial discharge source with respect to the acoustic sensor was considered. In order to study the effect of insulation aging on the ability to detect the partial discharge activity, the new oil was replaced by aged oil. Furthermore, a larger tank size was used in PD generation and the acquired acoustic PD signals were used to test the generalization capability of the neural network

3.1.1. New oil:

In this case, the acoustic sensor was mounted in position A as described in section 2.1. The samples were acquired at two different voltage levels, at 2.5 kV where no partial discharge activity was recorded and at 2.65 kV where the partial discharge signal was first observed. Typical acoustic signals with and without PD in addition to their wavelet decomposition levels are shown in Figure 15.

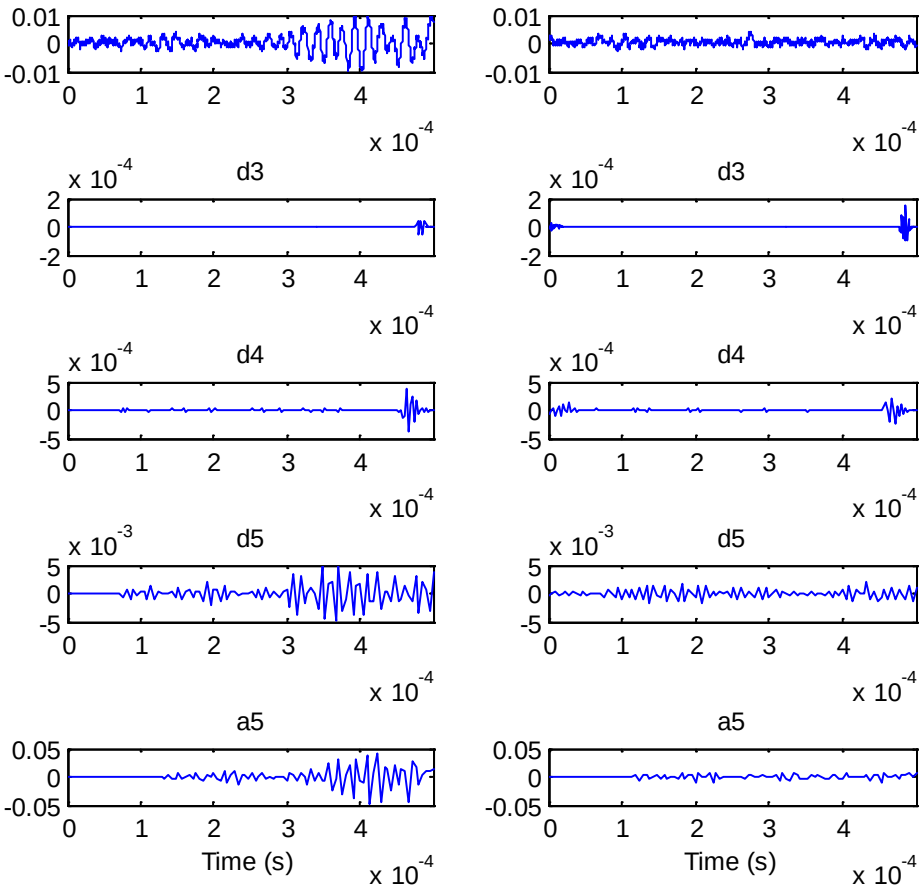

Figure 15: Typical acoustic signals with their wavelet decomposition, (new oil at position a) (a) with PD (b) with no PD

By analyzing the different wavelet scales for the two signals, it can be observed that the values of the wavelet coefficients for the acoustic PD signal at levels 4 and 5 are higher compared to the same levels of the acoustic signal with no PD. This corresponds to higher energy values for levels 4 and 5 of the analyzed acoustic PD signal. Moreover, by examining the approximation scales for the two signals, it can be noticed that there are more variations around the mean value in case of the acoustic signal with PD which leads to higher variance value.

The acoustic PD signal and acoustic signal with no PD are also analyzed based on their data distribution. The histograms of the acoustic signals with PD and with no PD are shown in Figure 16.

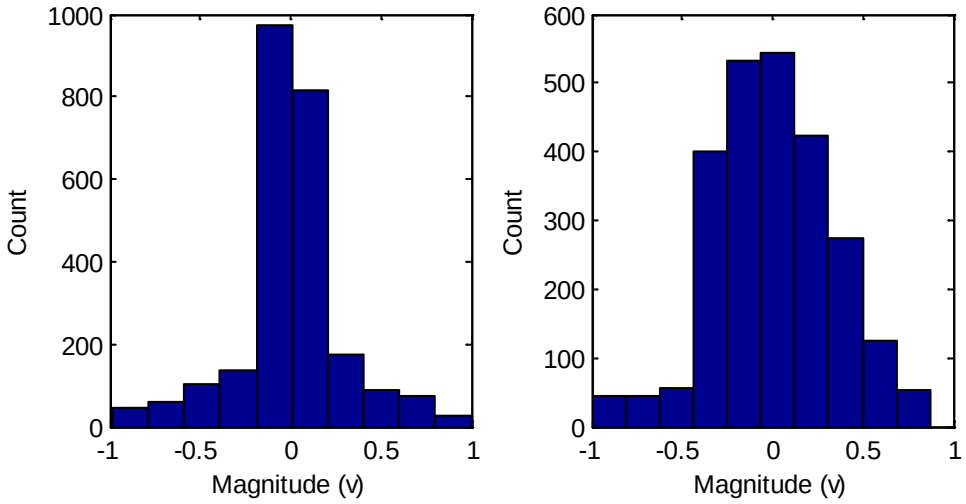

(a) (b)

Figure 16:Histogram of a typical acoustic signal , (new oil at position a), (a)with PD (b) with no PD

By inspecting the two histograms, it can be observed that the distribution of the AE signal is much more concentrated around the mean value. The Kurtosis measures the 'sharpness' in the data distribution, which is shown to be much greater in the case of PD signal. This is unlike the acoustic signal with no PD where the histogram is flatter and it is closer to a Gaussian distribution. In addition, the distribution of the no PD signal has some negative skewness while the distribution of the acoustic PD signal is more symmetric.

The frequency spectra for the acoustic signal with PD and with no PD are shown in figure 17.

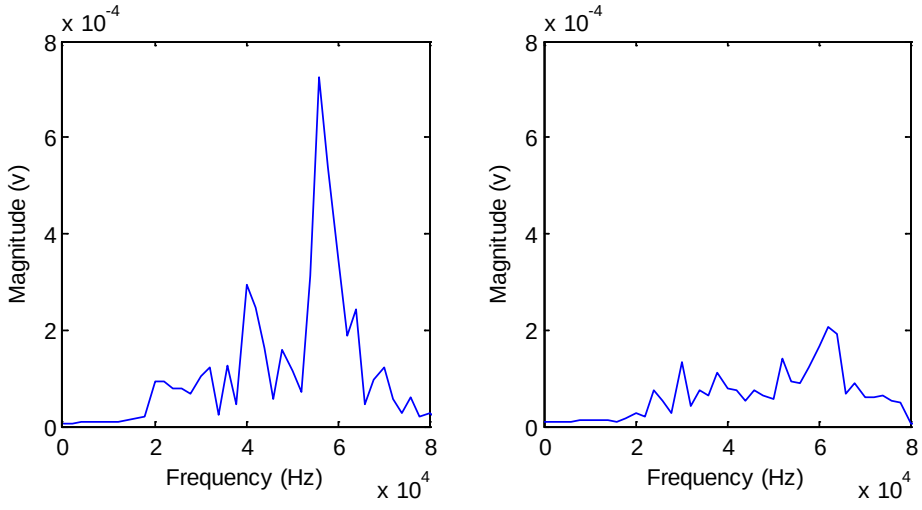

(a) (b)

Figure 17:Frequency spectrum of typical acoustic signals ,(new oil at position a) (a)with PD and (b)with no PD

Based on the two spectra, it can be seen that most frequency components in the spectrum of the acoustic PD signal have higher magnitudes relative to the spectrum of the acoustic signal with no PD. For this case, the dominant frequencies in the spectrum of the PD signal are in the range of 54-60 kHz.

Training and testing of the neural networks were based on the four types of features described in section 2.2. The recognition rates obtained for this case are shown in Table 5.

Table 5: Recognition rates for PD in new oil

Features	Recognition Rate (%)
Sub-band Variances	100%
Sub-band Entropies	98%
Kurtosis and Skewness	98%
FFT	100%

The recognition rates obtained using the different types of features were close to 100%. Such high recognition rates indicate that there is a strong correlation between the extracted features and the ability to detect the acoustic partial discharge signals in new oil. For example, when analyzing the wavelet coefficients of the acoustic signals with and without PD as shown in Figure 15, it can be seen that the energy level of the acoustic PD signal is higher at levels 4 and 5, which resulted in higher entropy value for those levels compared to the same wavelet levels of the acoustic signal with no PD. Also, analyzing the histograms of the acoustic signals with and without PD shown in Figure 16, demonstrates distinct difference between the two signals in terms of the kurtosis and skewness measures. The PD signals have higher kurtosis value in this case. In addition, by inspecting the frequency spectra of the two signals shown in Figure 17, it can be noticed that the magnitude of most frequency components in the spectrum of the PD signal is greater as compared to the spectrum of acoustic signal with no PD. It is worth mentioning that the kurtosis and skewness measures were evaluated for the original signals since it was found that using skewness and kurtosis of wavelet sub-bands produces lower recognition rates.

3.1.2. New oil with Paper Insulation:

The PD source and the acoustic sensor were fixed in the same positions as in the previous case, while a paper insulation sheet was inserted between the PD source and the acoustic sensor. The data was acquired at two voltage levels: 2.55 kV where there was no PD activity and at 2.75 kV where the PD activity was detected. The waveforms of the acoustic PD signal and the acoustic signal with no PD were similar to those obtained in case 1. The resulting recognition rates for this case are shown in Table 6:

Table 6: Recognition rates for PD in new oil with paper insulation

Features	Recognition Rate (%)
Sub-bands Variances	100%
Sub-bands Entropies	100%
Kurtosis and Skewness	96%
FFT	98%

Similar to the previous case with no barrier, the different types of features have produced high recognition rates. Based on this, it can be concluded that the presence of paper insulation did not affect the propagation of the acoustic signal and it did not cause significant attenuation for the acoustic PD signals that could have altered the classification performance. This could be due to the fact that there was no significant change in the acoustic impedances in the medium because the paper insulation was impregnated with oil.

3.1.3. New oil with metallic barrier:

The paper insulation sheet was replaced with a metallic barrier made of the transformer core material as shown in Table 7. The experiment was conducted with voltage levels of 2.4 KV (no PD activity) and at 2.6 KV (inception voltage level). The acquired acoustic PD signals are similar to those in cases 1 and 2. The recognition rates obtained for this case are summarized in Table 7.

Table 7: Recognition rates for PD in new oil with metallic barrier

Features	Recognition Rate (%)
Sub-band Variances	97%
Sub-band Entropies	100%
Kurtosis and Skewness	90%
FFT	98%

Except for the kurtosis and skewness measures which resulted in slightly less recognition rate than the previous cases, all other features have produced high recognition rates similar to those in case 1 and 2. The decrease in the recognition rate obtained for the skewness and kurtosis measures can be explained by knowing that the metallic barrier was not completely stable. In fact it was producing some vibrations which could be detected by the acoustic sensor. The presence of those vibrations in the acoustic signal with no PD resulted in similar data distributions to the signals with PD activity. Hence, for some cases the kurtosis and the skewness measures for the acoustic signals with and without PD were comparable. Apart from that, the presence of metallic barrier did not influence the detection ability of acoustic PD signal.

3.1.4. Changing the source location:

In this experiment, the location of the PD source was changed in order to investigate the effects of the travelling distance on the acoustic PD signals. The PD source was shifted to position b as described in section 2.1. In actual measurements, a mesh of acoustic sensors will be mounted on the transformer tank to account for the different propagation paths for the acoustic signal and the different attenuation factors.

The samples were acquired at 2.6 kV where PD was first recorded and at 2.4 where there was no PD activity. Typical acoustic signals with and without PD in addition to their wavelet coefficients are shown in Figure 18.

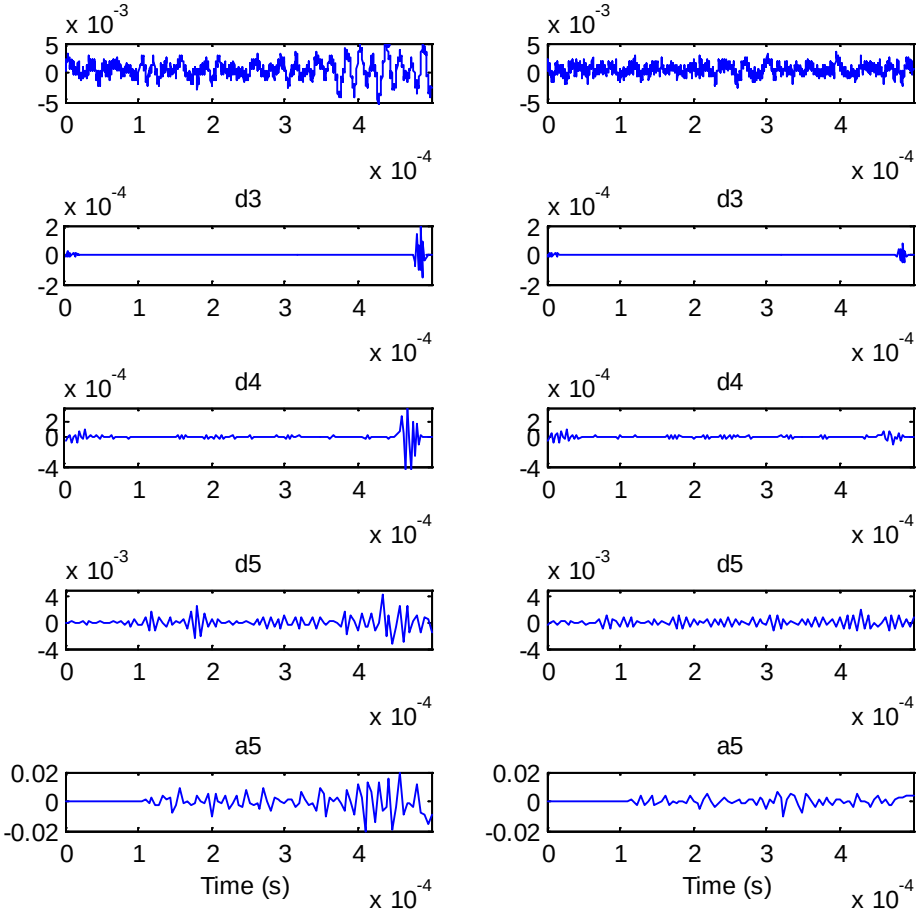

Figure 18: Acquired acoustic signals with their wavelet coefficients (new oil at position b) for (a) PD signal and (b) no PD signal

In this case, the propagating acoustic emission signal suffered from larger attenuation due to the relatively long travelling distance. This can be clearly observed when comparing the approximation coefficients of the PD signal to the case 1 where the PD source was located in position a as shown in Figure 15. There was a significant reduction in the magnitudes of the approximations coefficients when the PD source was shifted to position b. In addition, the signal variations around the mean values are comparable for the different wavelet scales of the acoustic signals with and without PD, except for level d4 and a5 in this case. For the above shown signals, there is more concentration of the acoustic PD signal in levels 4 and 5 relative to the acoustic signal with no PD which resulted in higher entropy values for those levels. The distribution of the entropy values in the two dimensional feature space for levels a5 and d5 is shown in Figure 19.

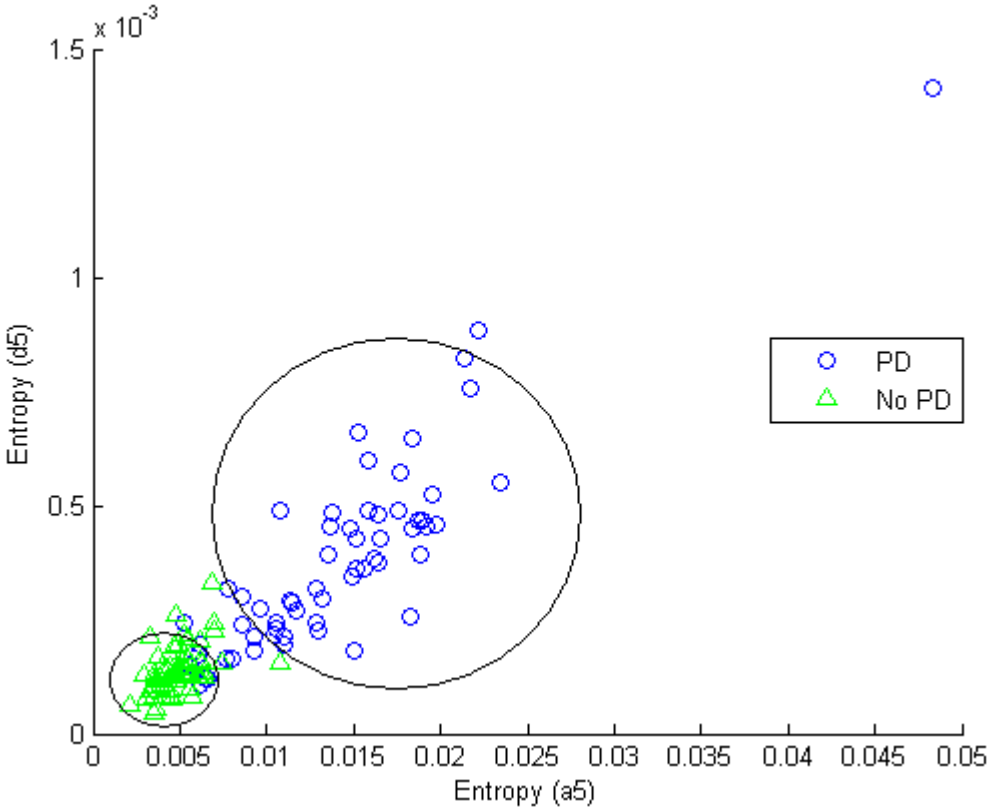

Figure 19: Sub-band entropies distributions for acoustic signals with and without PD, (new oil at position b)

Figure 19 shows that the values of the sub-band entropies for the acoustic signal with and without PD are mostly falling in two different clusters. Thus, the sub-band entropies have good discriminating ability between the two classes in this case.

The histograms of the acoustic signals with and without PD are shown in Figure 20.

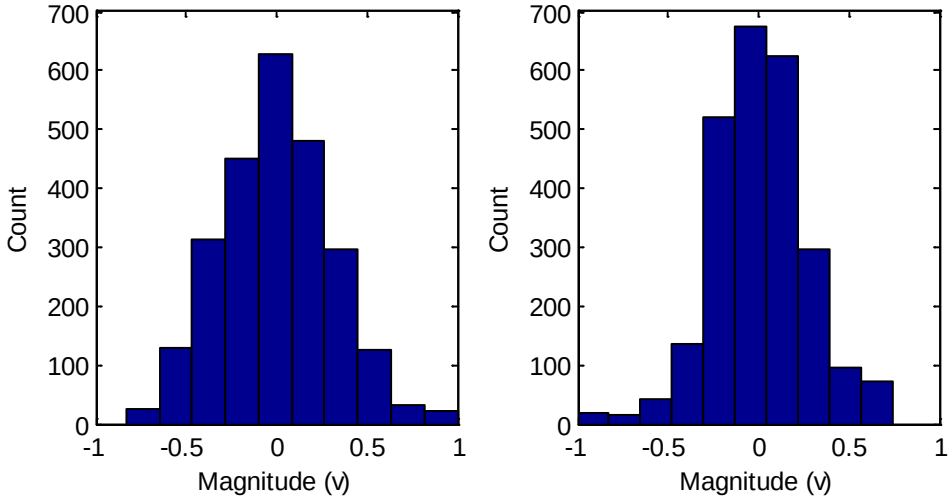

Figure 20: Histogram of acoustic signals (new oil at position b) (a) PD signal (b) no PD

The histogram of the acoustic PD signal is flatter than in case 1. Due to the large attenuation, the magnitude of the acquired PD signal is closer to the magnitude of the background noise and the values are more distributed. This generally resulted in less kurtosis values for the acoustic PD signals in this case relative to case 1. When examining the skewness measure, it can be seen that the two histograms are almost symmetric around the mean, thus the skewness measure is close to zero for both signals. The distribution of the skewness and kurtosis values in the 2-D feature space for the acoustic signal with and without PD is shown in Figure 21

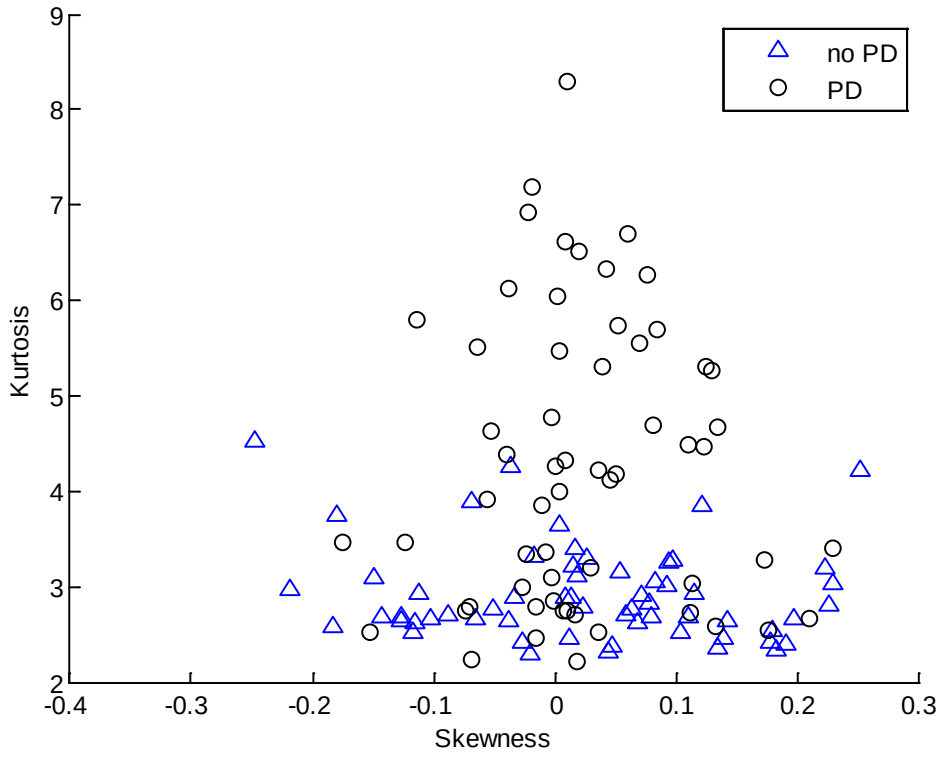

Figure 21: Ditstributions of kurtosis and skewness measres foracoustic signal with and with out PD, (new oil, position b)

Unlike the distribution of entropy values, the values for skewness and kurtosis measures for the two classes are mostly overlapping. This shows that the skewness and kurtosis measures have high sensitivity to the level of the acoustic signals and the amount of attenuation.

The frequency spectra of the PD signal and the no PD are shown in Figure 22.

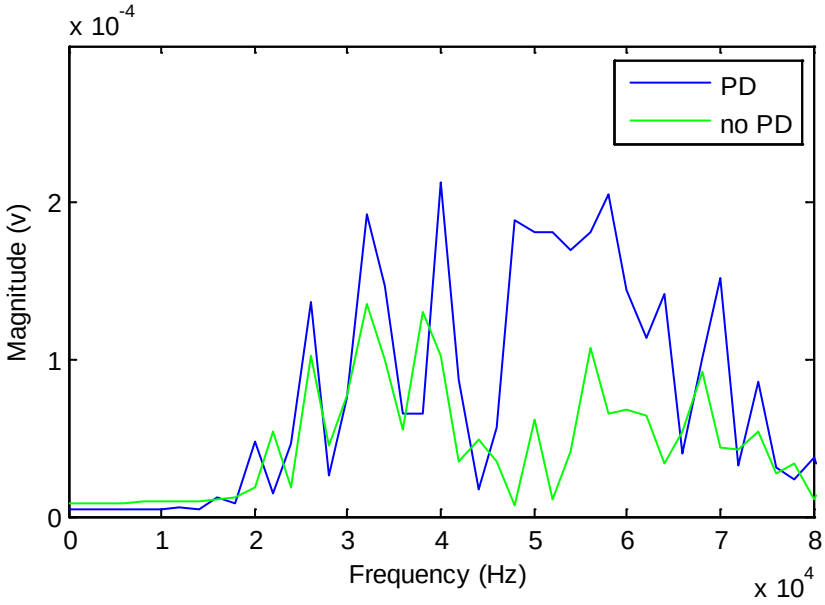

Figure 22: Frequency spectrum of acoustic signals (new oil at position b) with and without PD

There is clear attenuation for the different frequency components. The energy in the two spectra is also comparable. However, it can be noticed the magnitude of the frequency components in the range 50-60 kHz is higher in the spectrum of the acoustic PD signal.

The recognition rates obtained in this case for the different types of features are summarized in Table 8.

Table 8: Recognition rates for PD-position b

Features	Recognition Rate (%)
Sub-band Variances	85%
Sub-band Entropies	90%
Kurtosis and Skewness	70%
FFT	80%

There is a significant drop in the recognition rates obtained in this case compared to previous cases. This is mainly due to the long propagation distance, which causes more attenuation for the acoustic signals. Moreover, since PD source was placed close to tank side, the effect of reflections and interference became more apparent. Table 8 shows that highest recognition rate was obtained using the sub-band entropies. This is because of the greater concentration of acoustic PD signal in

certain wavelet sub-bands relative to the acoustic signal with no PD as shown in Figure 19. It can be also noticed that the values of the sub-band entropy for the two classes were grouped in two different clusters. Thus, using the sub-band entropies has better detection performance in this case. On the other hand, the kurtosis and skewness measures produced the lowest recognition rates. This is because of the greater similarity between the data distributions of the acoustic PD signal and the acoustic signal with no PD as represented in Figure 20. Using the FFT coefficients produced good accuracy rate (80%). By inspecting the frequency components in the spectra of the two signals in Figure 22, it can be observed that the frequency components in the PD spectrum have greater magnitudes. Figure 23 shows the percentage of false alarms and false positives produced for the different types of features:

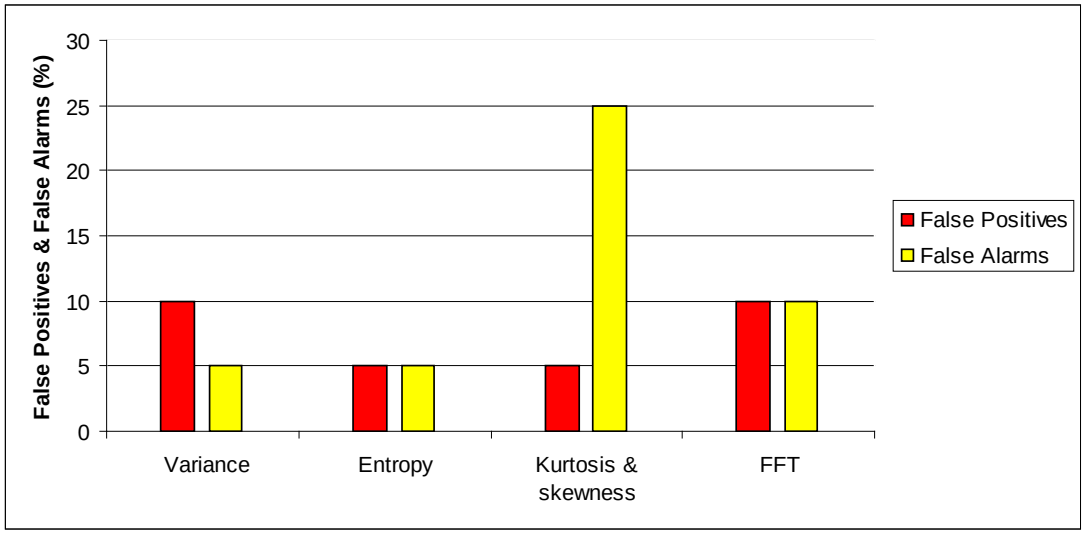

Figure 23: Evaluation of PD detection with the sensor located in positin b

The highest percentage of false alarms was produced when using the kurtosis and skewness measures, while the sub-band variances and the FFT coefficients resulted in high false positives rate.

3.1.5. Old oil:

The new oil was replaced with aged oil. The point here is to study the effect of the status of transformer oil, as insulation medium, on the partial discharge signal and hence on the detection of PD signals. The samples were acquired at two different voltage levels, at 2.00 kV where no partial discharge signal was recorded and at 2.35 kV which was the inception voltage of the PD activity. The inception voltage of the PD signal was less than previous cases due to the degradation in the insulating

properties of the old oil. Figure 24 shows typical acoustic signals with and without PD activity in addition to their wavelet decomposition.

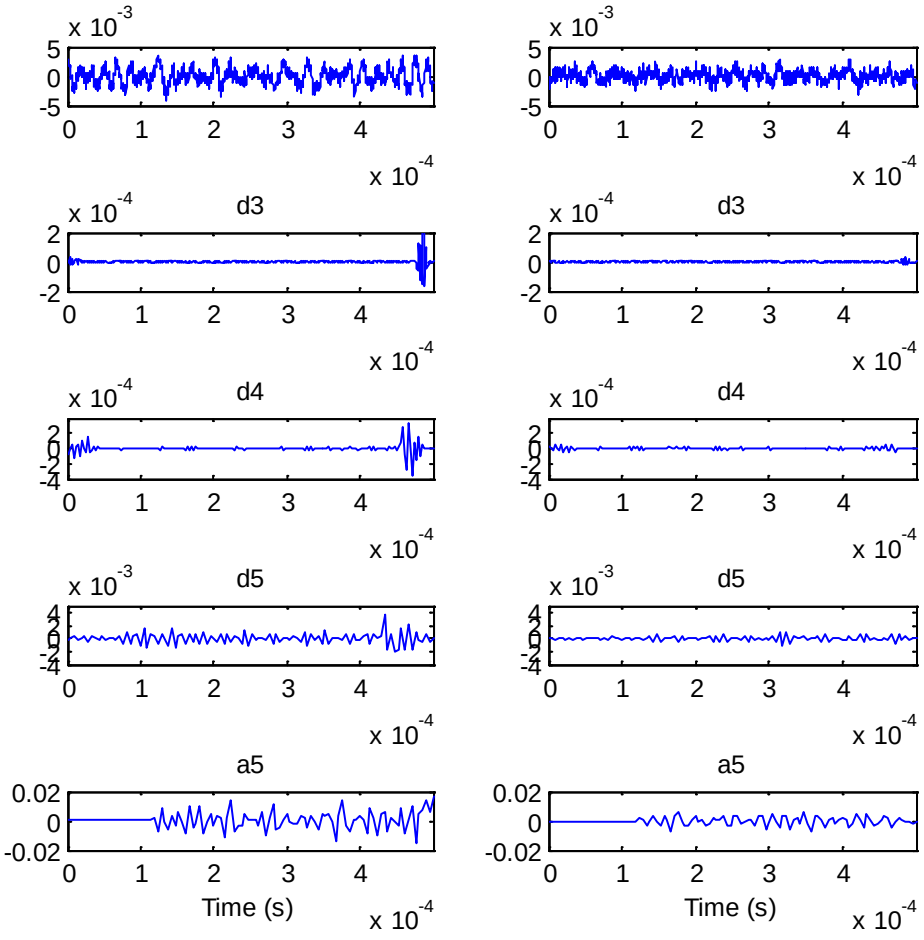

Figure 24: Acoustic signal and their wavelet coefficients (old oil) (a) PD signal (b) no PD

By comparing the different wavelet levels of the two analyzed signals, it can be noticed that there are greater variations around the mean values in case of the acoustic PD signal. Additionally, the wavelet coefficients of the acoustic PD signal at levels 3 to 5 have greater magnitudes than the coefficients at the same scales of the signal with no PD. This means that the energy of the PD is more concentrated in these levels which correspond to higher entropy values in this case. Figure 25 illustrates the distribution of the entropy values in the 2-D feature space for the acoustic signals with and without PD.

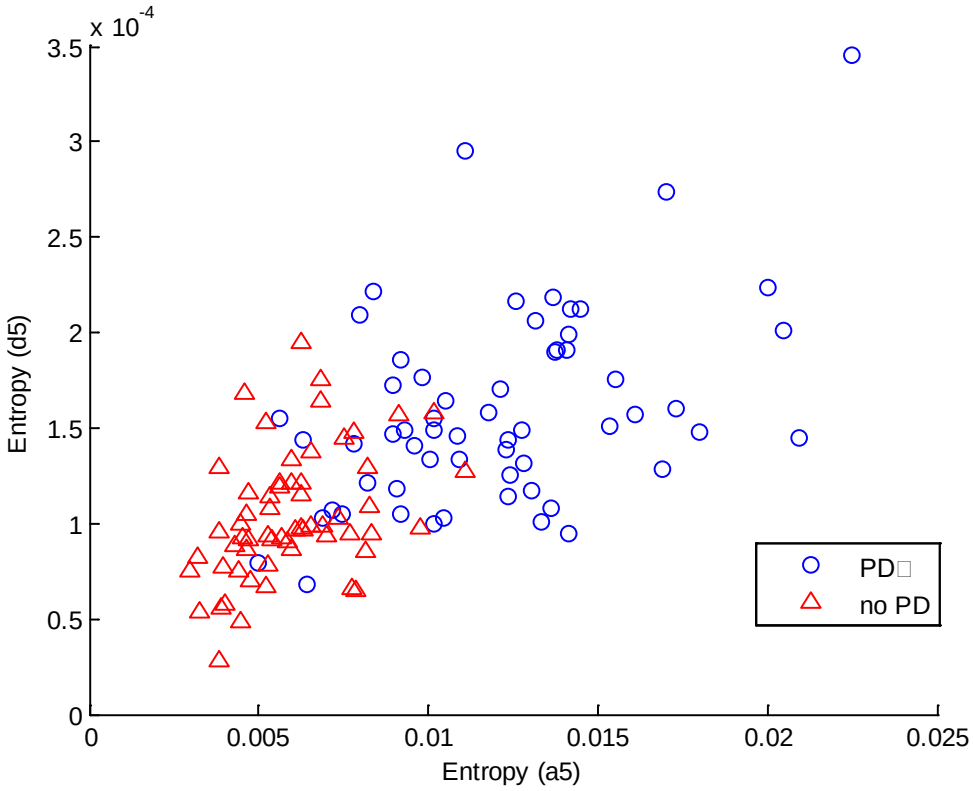

Figure 25 : Sub-bands entropy distributions for acoustic signals with and without PD, (old oil)

It can be seen that the amount of overlap between the two classes is relatively small. In fact, except for few signals, most of the PD signals have higher sub-band entropies values compared to signal with no PD. This shows that the sub-band entropy is a discriminating feature between the two classes.

The histograms of the acoustic signal with and without PD are shown in Figure 26:

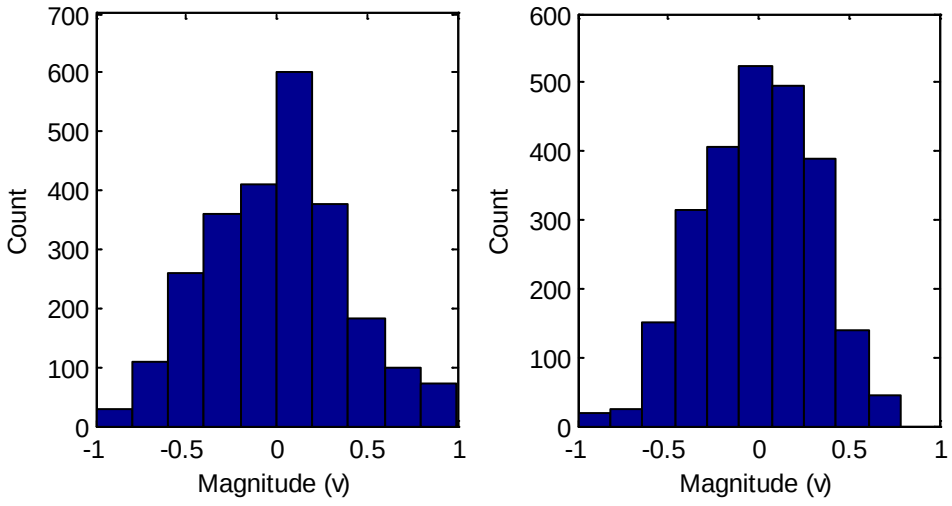

(a) (b)

Figure 26: Histogram of acoustic signals (old oil) (a) with PD (b) no PD

By inspecting the histograms of the two signals, it can be noticed that both distributions have similar sharpness which indicates that the kurtosis values of the two signals are comparable. Also the two histograms are symmetric around the mean value which corresponds to zero skewness for both signals. The distribution of the skewness and kurtosis measures for the acquired signal in the 2-D feature space is shown in Figure 27:

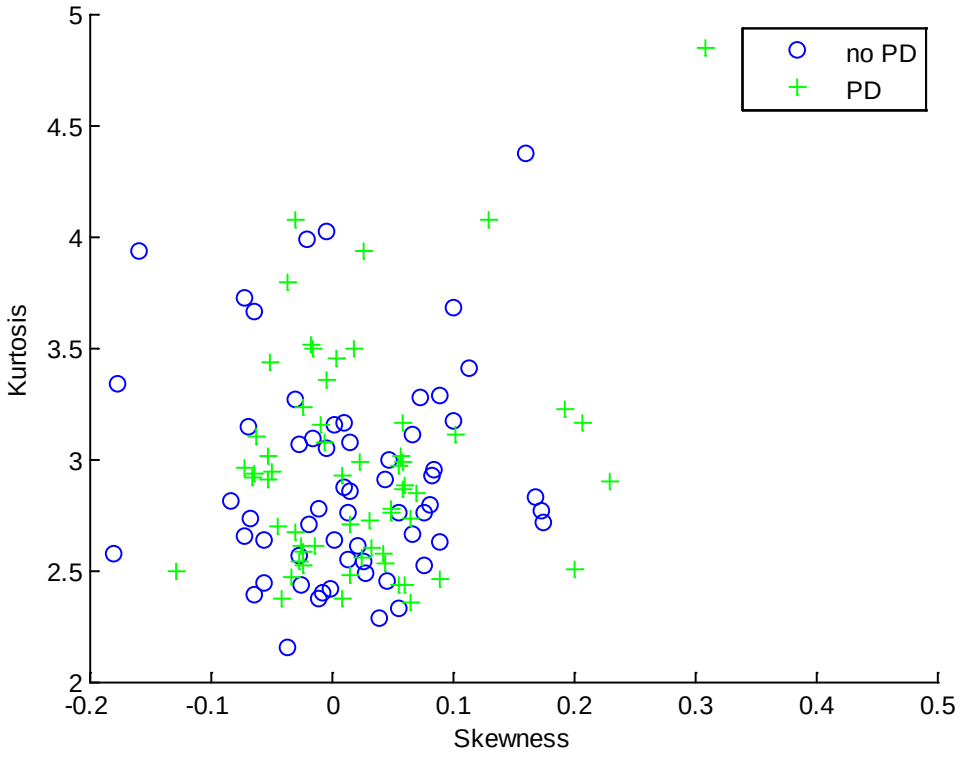

Figure 27: Distributions of kurtosis and skewness measures for acoustic signal with and without PD, (old oil)

The skewness and kurtosis values for the two classes are completely overlapping. Most signals have zero skewness and kurtosis of 3 which is equivalent to Gaussian distribution. Thus, the statistical measures have poor discriminating ability in this case.

The frequency spectra of the acoustic PD signal and the acoustic signal with no PD are shown in Figure 28.

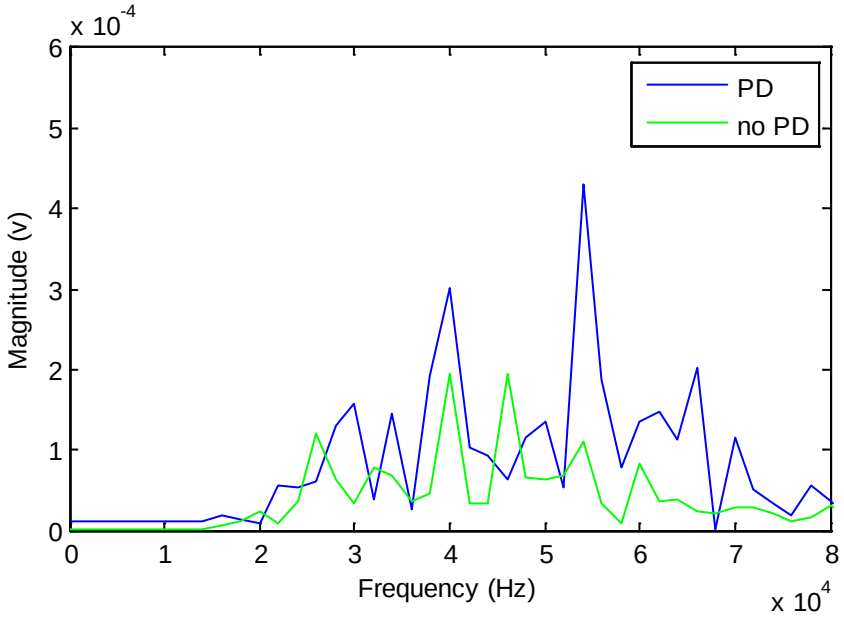

Figure 28: Frequency spectrum of acoustic signals with and without PD , (old oil)

In this case, the dominant frequencies of the acoustic PD spectrum are in the range of 54-58 kHz. Also, compared to case 4 (PD source in position b), there is less attenuation for the different frequency components in the spectrum of the PD signal in this case.

The recognition rates obtained in this case are summarized in Table 9:

Table 9: Recognition rates for PD-old oil

Features	Recognition Rate (%)
Sub-band Variances	78%
Sub-band Entropies	88%
Kurtosis and Skewness	60%
FFT	82%

The sub-band entropy measure produced the highest recognition rate (around 88%), while the rest of features resulted in less classification rates. The values of the sub-bands entropy for the acoustic PD signal were generally higher than those of the acoustic signal with no PD as illustrated in Figure 25. The lowest recognition rate was obtained using kurtosis and skewness measures. Because of the high attenuation, the values of the PD signal were very close to the background noise. Thus, there is high similarity between the histograms of the acoustic signals with and without PD

as demonstrated in Figure 26. Hence the values of the kurtosis and skewness measure were comparable for the two signals. In fact, the old oil used has greater density than new oil. This is mainly because of the presence of some by-products that resulted from the degradation in paper insulation. The density of old oil is directly proportional to the acoustic impedance as dictated by Equation 1. Hence, old oil has greater acoustic impedance than new oil which affected the detection performance in this case. In order to improve the recognition rates, the different features were also used in combinations but there was no significant improvement in the recognition rates.

The distribution of misclassifications due to false alarms and false positives is shown in Figure 29:

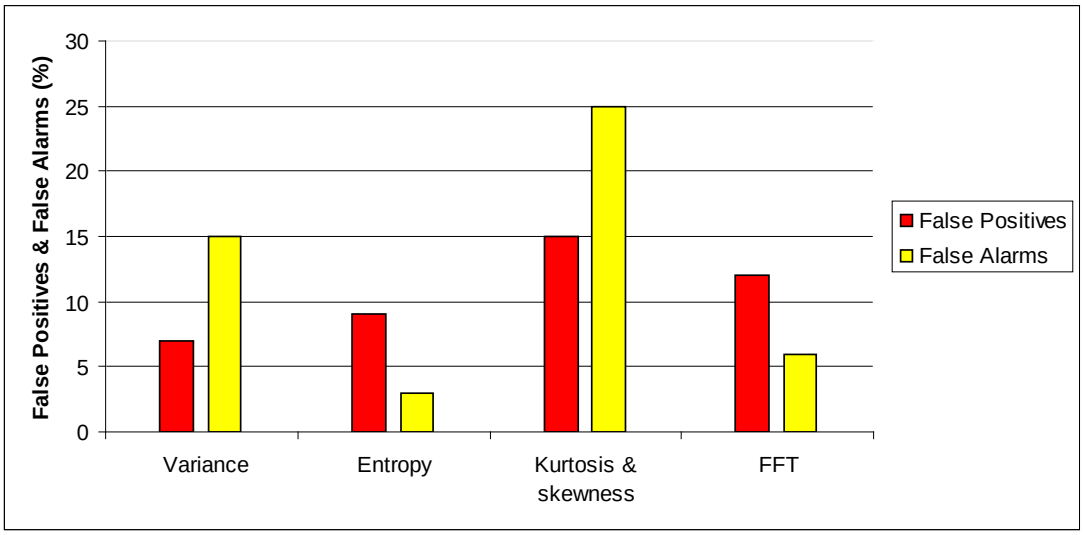

Figure 29: Evaluation of PD detection in old oil

Classification error was mainly due to false positives in the case of entropy. On the other hand, the kurtosis and skewness produced high false alarms.

3.1.6. Big Tank:

In this case, the effect of the tank size on the ability to detect the acoustic partial discharge signal was investigated. Another tank with larger dimension was used. Typical acoustic signals with and without PD activity and their wavelet coefficients are shown in Figure 30.

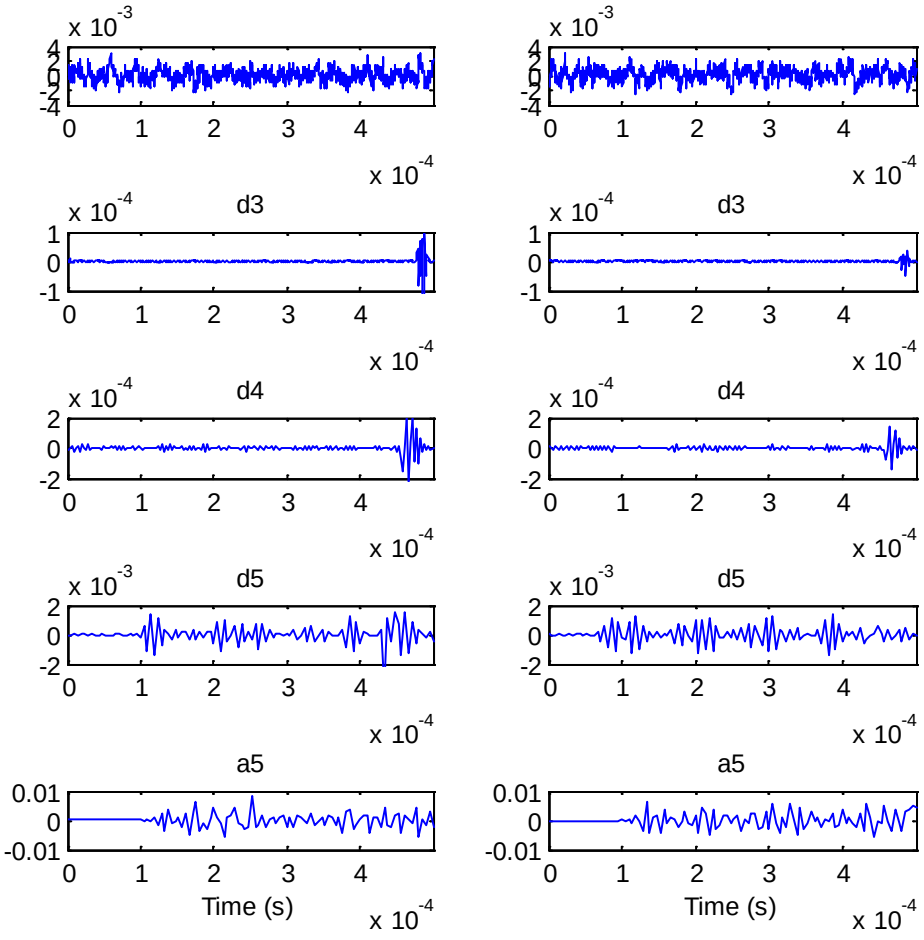

Figure 30: Acoustic signal and their wavelet coefficients, (big tank) for (a) PD (b) no PD

From the figure shown, it can be seen that due to the bigger tank size, the acoustic energy released during the PD activity was scattered over larger area. Thus, the detected PD signal using the acoustic sensor is highly attenuated compared to all previous cases. Also, it can be observed that the magnitudes of the wavelet coefficients for the two acoustic signals are comparable at the different decomposition levels. Moreover, there is similar amount of variations in both cases which means that the values of the sub-band variances are very close. The distribution of entropy values in the 2-D feature space for scales a5 and d5 is shown in Figure 31:

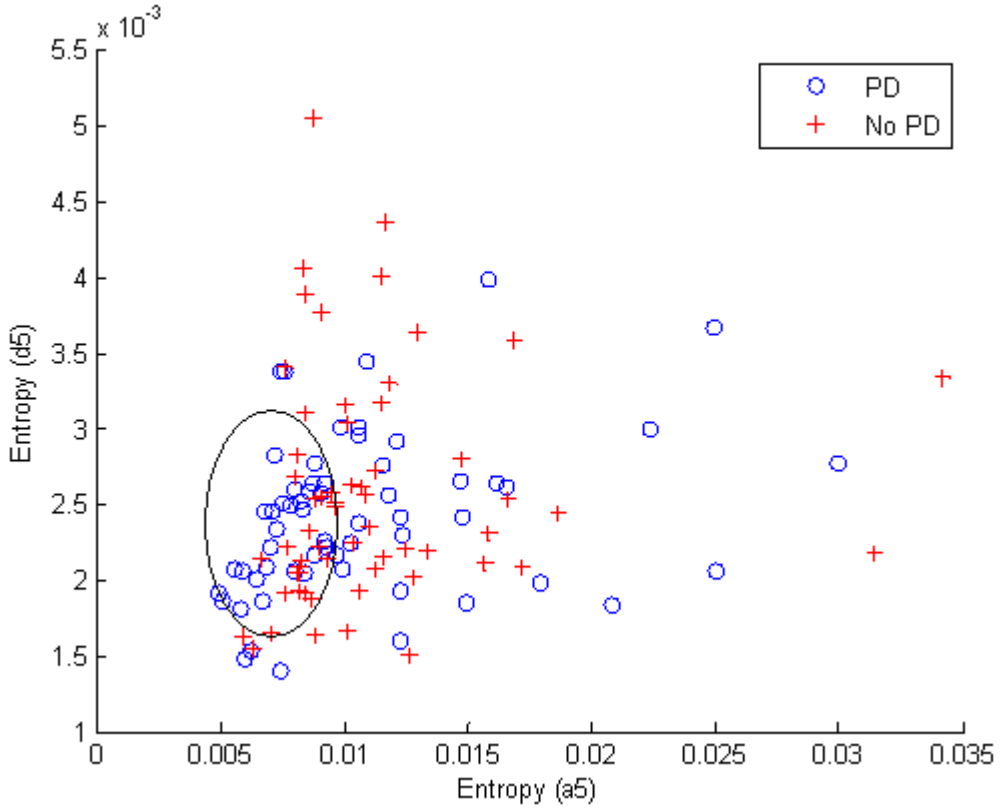

Figure 31: Distribution of sub-band entropies for acoustic signals with and without PD, (big tank)

Unlike the previous cases, most values of the sub-band entropies for the two classes are overlapping in this case. However, there is some concentration of entropy values for the PD signals as illustrated in Figure 31. This shows that there might be some correlation between the presence of PD signals and the values of the sub-band entropies.

The histograms of acoustic signal with and without PD are shown in Figure 32:

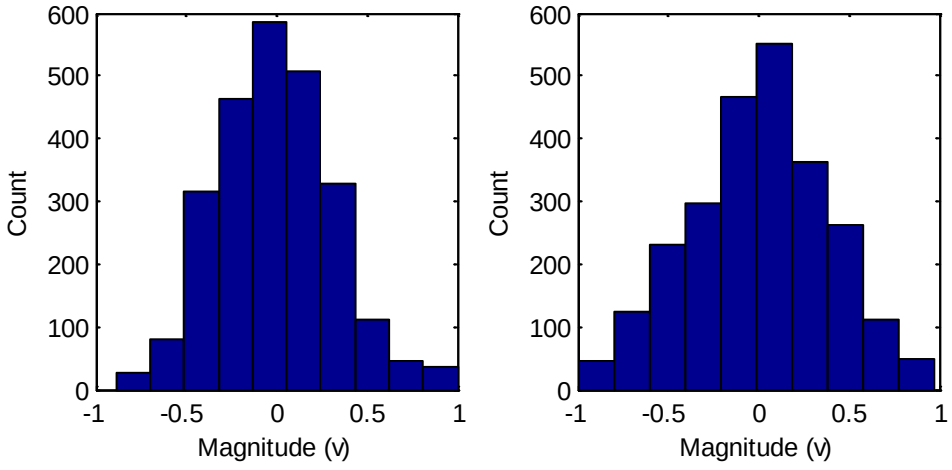

Figure 32: Histogram for acoustic signals (big tank) (a) PD signal (b) no PD

Due to the large attenuation, the distribution of the PD is much closer to the distribution of the acoustic signal with no PD. The two histograms have similar sharpness. The value of kurtosis measure for both distributions is around 3. The skewness is also comparable in both cases because the two distributions are almost symmetric around the mean value. The distribution of the skewness and kurtosis values in the 2-D feature space for the acoustic signals with and without PD is shown in Figure 33.

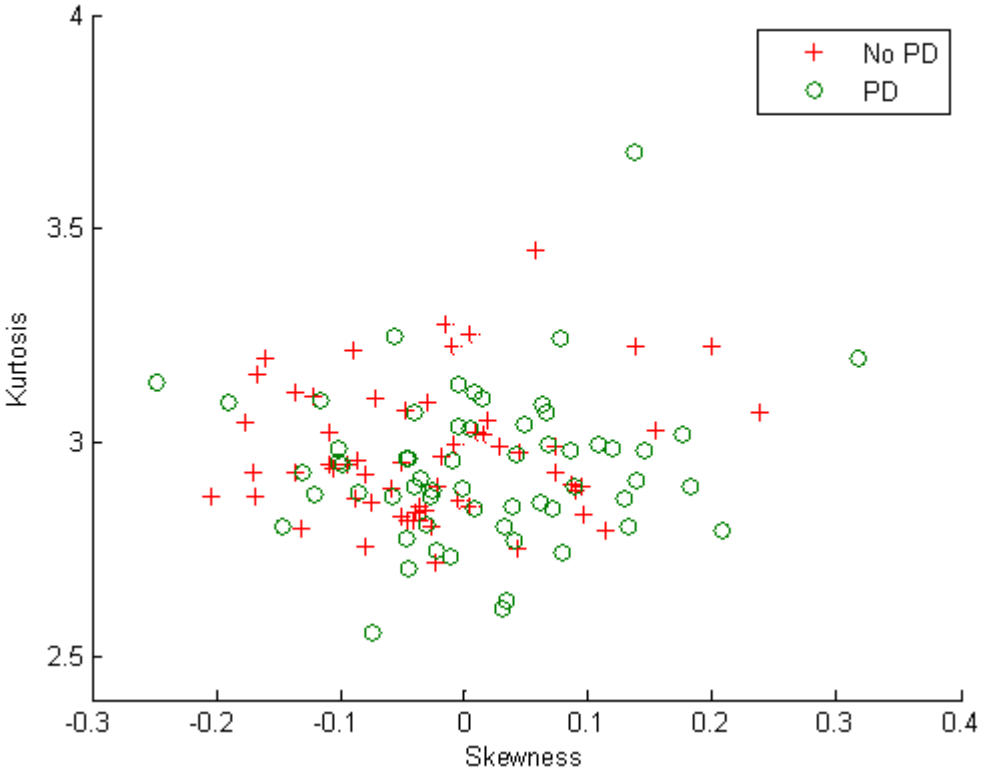

Figure 33: Distribution of kurtosis and skewness measures for acoustic signal with and with out PD, (big tank)

Similar to the previous two cases, the values of the skewness and kurtosis measures for the two classes are completely overlapping in this case. Thus, the skewness and kurtosis measures are not reliable features for PD recognition in this case as well.

The frequency spectra for the PD signal and the no PD are shown in Figure 34:

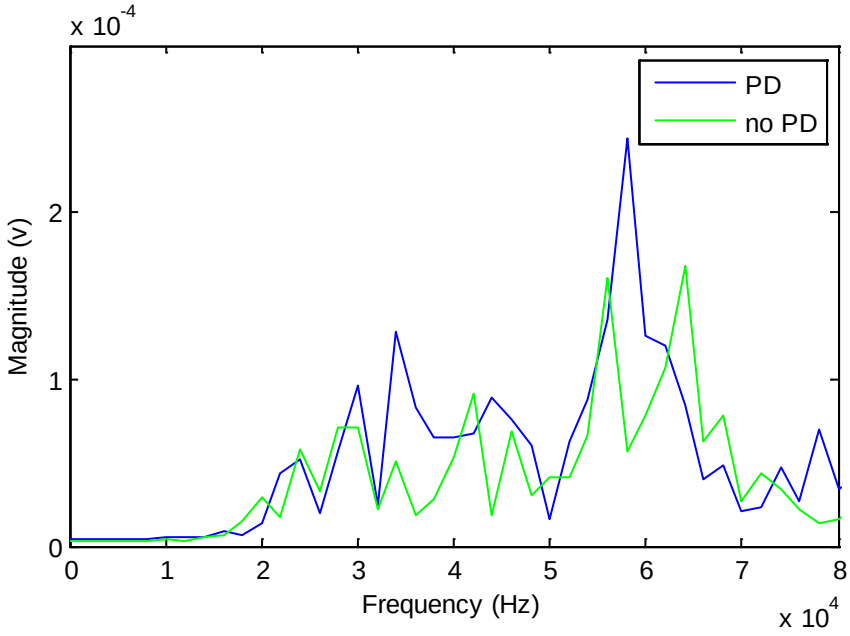

Figure 34: Frequency spectrum of acoustic signals (big tank)

Compared to all previous cases, the different frequency components in the spectrum of the PD signal were much more attenuated in this case. The energy levels of the two spectra are comparable.

The signals acquired in the big tank experiment were used for training and testing the neural network. The resulting recognition rates are shown in Table 10:

Table 10: Recognition rates for PD-Big tank

Features	Recognition Rate (%)
Sub-bands Variances	50%
Sub-bands Entropies	78%
Kurtosis and Skewness	54%
FFT	65%

It can be observed that using the sub-band entropies resulted in the highest recognition rates (around 78%). This shows that there is a stronger correlation between the sub-bands entropy and the ability to detect PD signals. The recognition rate obtained using the sub-band variances was 50%. By analyzing the wavelet decomposition levels, shown in Figure 30, it can be seen that the coefficients

variations are comparable for both cases. Using the FFT coefficients produced an accuracy rate of 65%. As can be observed in Figure 34, the spectra of the two signals have similar magnitudes for the different frequency components. Figure 35 shows the false alarm rate against the false positives rate for the different features used:

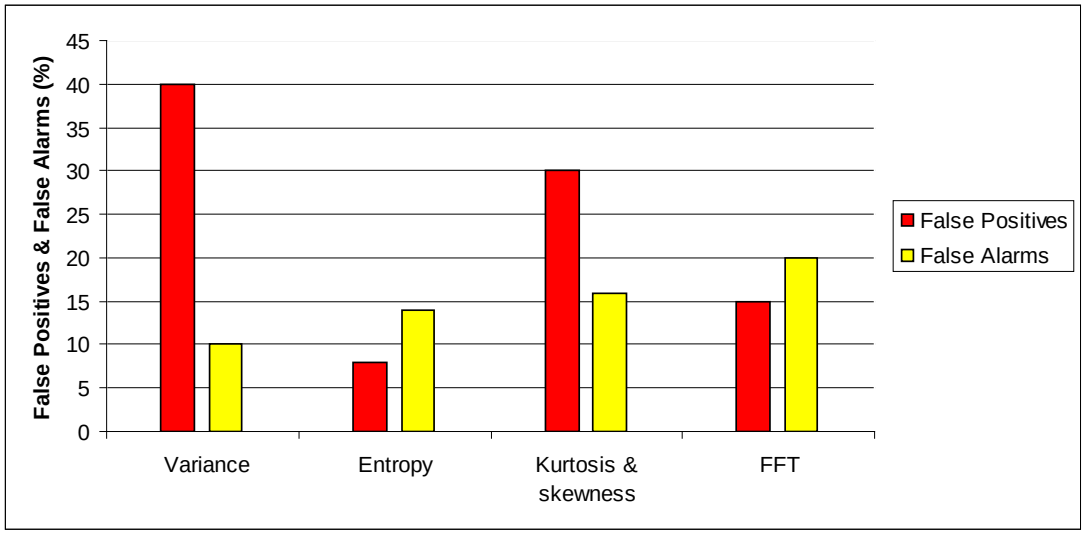

Figure 35: Evaluation of PD detection in new oil (big tank)

The rate of false positives reached its maximum when using the statistical features (variance, kurtosis, skewness). While using the sub-band entropies measure, the classification error was mainly due to false alarms.

In order to check the generalization ability of the trained neural network for completely new cases, the training was done using the samples from a previous experiment (case 1), and the neural network was tested with acquired signals in the big tank experiment. The recognition rates obtained are shown in Table 11:

Table 11: Recognition rates for PD-Big tank

Features	Recognition Rate (%)
Sub-bands Variances	50%
Sub-bands Entropies	50%
Kurtosis and Skewness	50%
FFT	45%

All types of features produced poor recognition rates in this case. This indicates that the values of the extracted features for the two cases (big tank and small tank) are mostly falling in two different ranges.

3.2. Assessment of Transformer Oil Condition

In this part, the effect of the transformer insulation aging on the partial discharge signal was studied. Since the acoustic emission signal is a mechanical wave, its propagation is affected by the status of the medium. By knowing what features of the partial discharge are more affected when the transformer insulation is aged, it might be possible to predict the condition of the transformer oil based on the value of those features. Usually when the transformer oil is aged, it becomes less homogenous because of the higher percentage of water content and the particles resulted from chemical reaction because of heating (through overloading, short circuit or due to the partial discharge activity). For this case, features were extracted from the PD signal that occurred in both types of oil and fed to the neural network. The samples were acquired at 2.35 kV for the old oil and at 2.6 kV for the new oil. Typical acoustic PD signal obtained in new and old oil and their wavelet coefficients are shown in Figure 36.

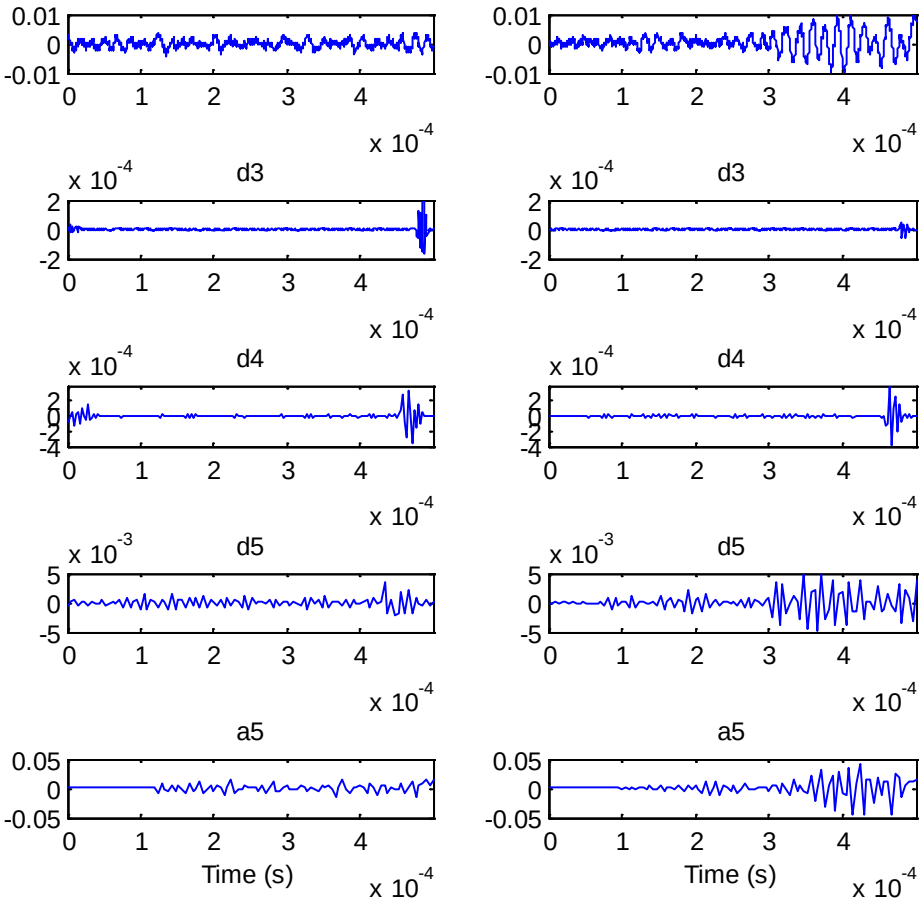

(a) (b)

Figure 36: Acoustic PD signal and their wavelet coefficients in (a) old oil (b) new oil

There are more variations in the magnitudes of the wavelet coefficients for the acoustic PD signal in new oil, especially for the details and approximation signals at level 5. Also, the signal energy is more distributed among the different wavelet levels in case of old oil while it is more concentrated in level 5 for the PD in new oil. This corresponds to a difference in the sub-band entropy measures for the two signals. The histograms of the PD signal in new oil and old oil are shown in Figure 37.

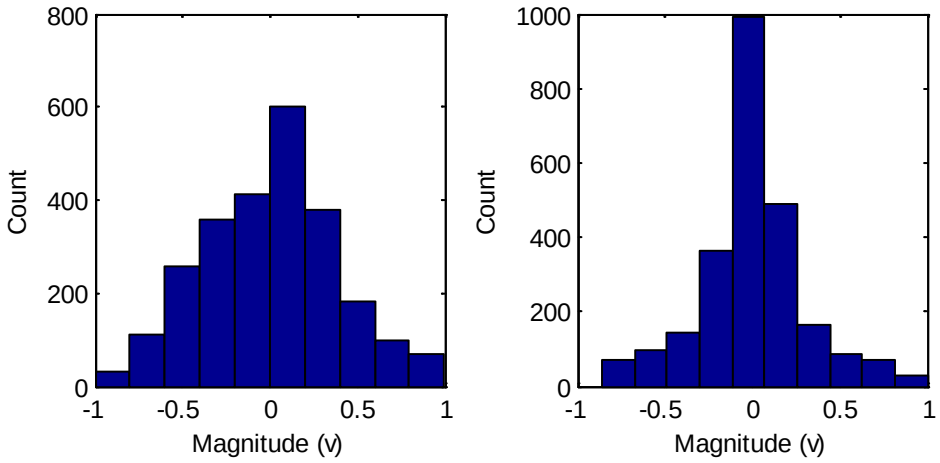

(a) (b)

Figure 37: Histogram for (a) old oil PD (b) new oil PD

The histogram of the PD in new oil has more sharpness and it is more concentrated, while the histogram of the PD signal in old oil is flatter and the data is more distributed. This resulted in higher kurtosis value for the PD signal in new oil in this case. Furthermore, the two histograms are almost symmetric around the mean which indicates that skewness values for both signals are close to zero.

The frequency spectra of the PD signal in new oil and old oil are shown in Figure 38.

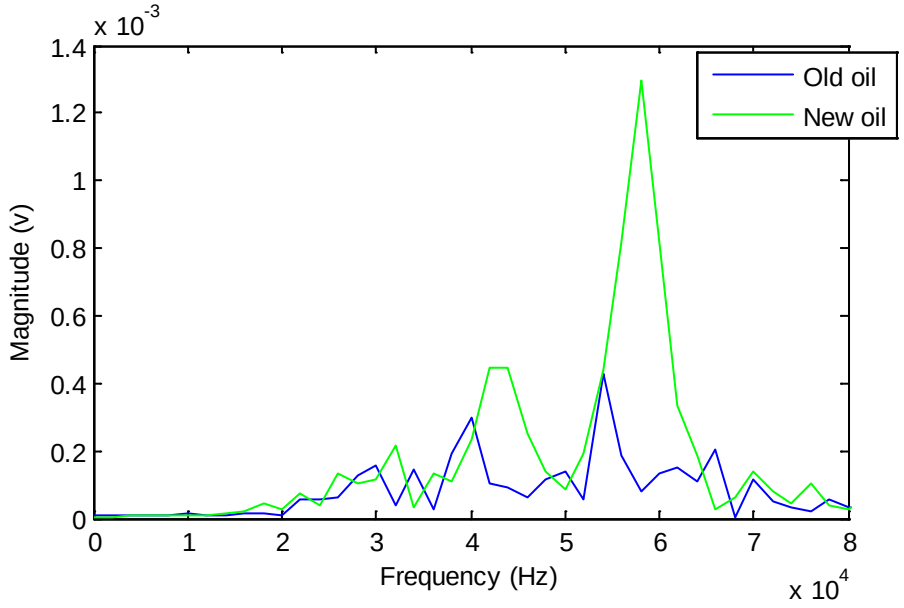

Figure 38: Frequency spectrum of PD signal in new oil and old oil

It can be observed that most of the frequency components in the spectrum of the PD signal in new oil have greater magnitudes as compared to the spectrum of PD in old oil. This due to the higher attenuation for PD signals in old oil.

The same features as in the previous part were used to construct the feature vectors for training the neural network. The recognition rates obtained are shown in Table 12:

Table 12: Recognition rates for PD in new oil and old oil

Features	Recognition Rate (%)
Sub-band Variances	95%
Sub-band Entropies	100%
Kurtosis and Skewness	90%
FFT	95%

High recognition rates were obtained (above 90%) for the different types of features used. Using the sub-band entropies measures produced a classification rate of 100%. By inspecting the wavelet coefficients of the two signals shown in Figure 36, it can seen that the wavelet coefficients of the PD signal in new oil have greater magnitudes and they are more concentrated which resulted in higher entropy values relative to the PD signal in old oil. The recognition rate obtained using the skewness and kurtosis measures was 90%. The histogram of the PD signal in new oil has more sharpness which means higher kurtosis value. On the other hand, by observing the two histograms shown in Figure 37, it can be noticed that the two distributions are almost symmetric, thus the skewness values for both signals are close to zero. The FFT coefficients also produced high recognition rate (95%). By comparing the two frequency spectra shown in Figure 38, it can be noticed that most frequency components in the spectrum of PD in new oil have greater magnitudes relative to the spectrum of PD in old oil. In fact, the acoustic PD signal in old oil was more attenuated because old oil has higher acoustic impedance than new oil.

3.3. Classification of PD source

Partial discharge signals can be generated either outside or inside the transformer tank. Even after attenuation, the magnitude of the corona discharges might be greater than PD signal generated in the transformer insulation because acoustic signals propagating in air are less attenuated. Thus, those external discharges could be acquired by the acoustic sensor and might be confused with PD signal which

occurred in transformer oil. The objective of this part is to compare between the external PD and the oil PD using the different types of features.

3.3.1. Old Oil PD and Air PD:

In this case, the features were extracted from the partial discharge signal within the old oil and the corona discharge. Figure 39 shows typical corona discharge signal and PD signal in old oil in addition to their wavelet decomposition (levels 3-5).

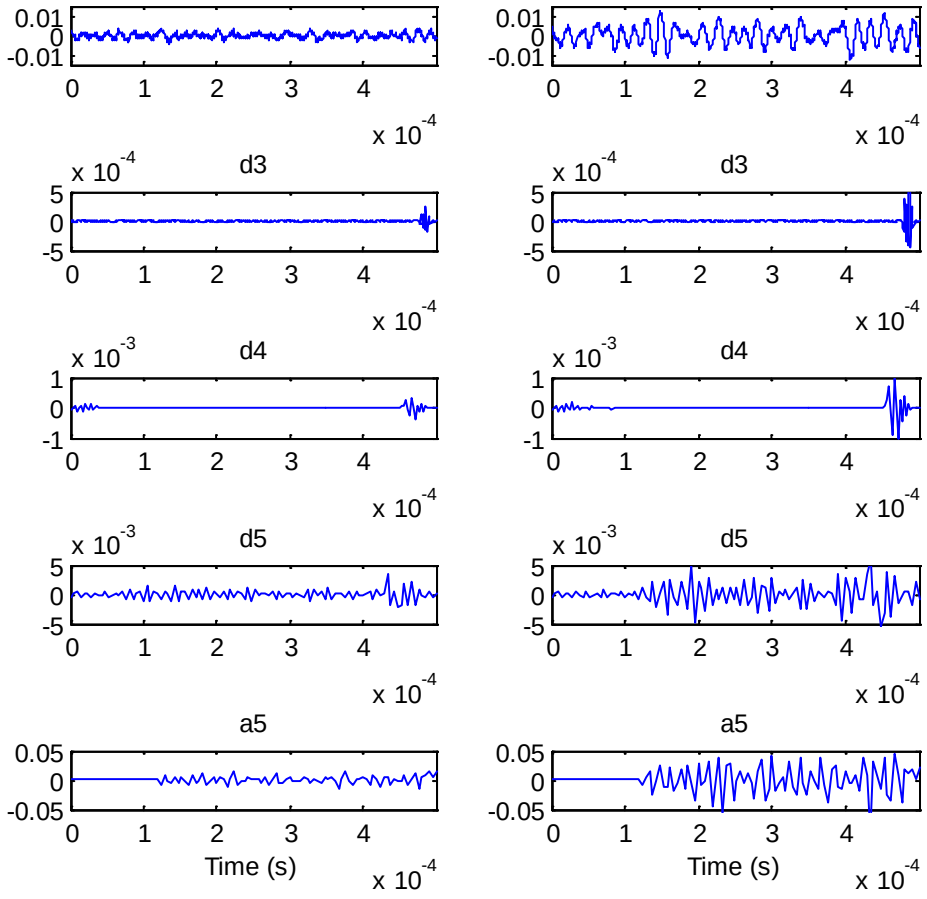

(a) (b)

Figure 39: Acoustic PD signal and their wavelet coefficients in (a) old oil (b) Corona

As can be seen in Figure 39, there are more variations in the magnitudes of the wavelet coefficients for the corona discharge signal especially at the different decomposition levels as compared to the same levels of the analyzed acoustic PD in old oil. Also, it can be noticed that the signal energy is more concentrated in level 5 in case of corona discharge which indicates that the values sub-band entropies are

greater for the corona discharge signal. The histograms of the PD in old oil and the corona discharge are shown in Figure 40:

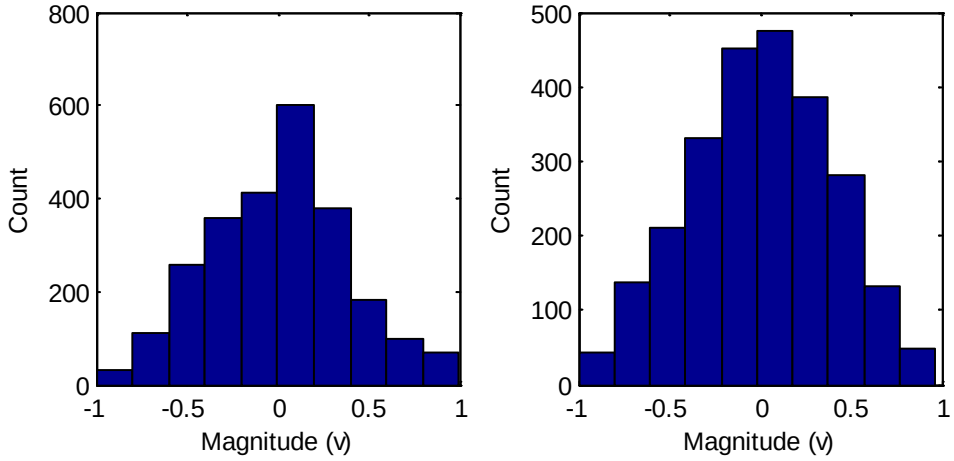

(a) (b)

Figure 40: Histogram for (a) old oil PD (b) Corona discharge signal

Both histograms have similar sharpness levels. Thus, the corona discharge signal has comparable kurtosis value with PD in old oil. On the other hand, the skewness value for the two distributions is close to zero, because they are almost symmetric around the mean.

The frequency spectra of the PD in old oil and the air PD are shown in Figure 42.

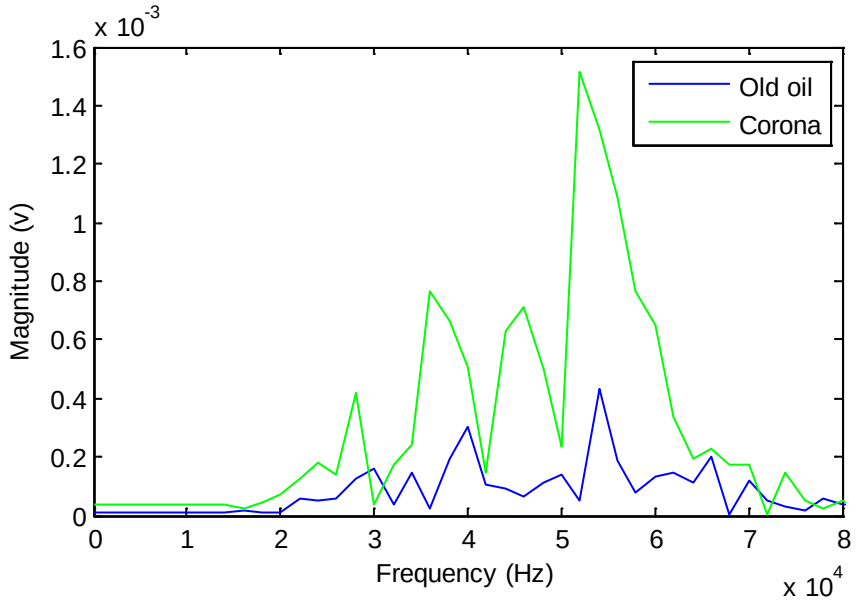

Figure 41: Frequency spectra of PD in old oil and Corona discharge signal

Based on the two spectra, it can be noticed that the different frequency components have greater magnitudes in case of corona discharge signal. This is mainly because PD signals propagating in air are less attenuated as compared to PD in old oil.

The output recognition rates using the different types of features are summarized in Table 13:

Table 13: Classification rates for PD in old oil and air PD

Features	Recognition Rate (%)
Sub-band Variances	98%
Sub-band Entropies	100%
Kurtosis and Skewness	65%
FFT	96%

In this case, all types of features have produced high recognition rates. This indicates that the extracted features have good discriminating ability between the two types of partial discharge. For example, the sub-band variances have produced a classification rate of 97%. By examining the wavelet analyzed signals shown in Figure 39, it can be noticed that there are more variations in the magnitude of the wavelet coefficients for the corona discharge signal which resulted in higher variance values relative to the PD in old oil. The skewness and the kurtosis measures produced a low recognition rate as compared to the sub-band variances. As shown in Figure 40, the histograms of the PD signal in old oil and the corona discharge have similar sharpness and they are both symmetric. Thus the kurtosis and skewness values were comparable for both signals.

3.3.2. New oil and Air PD:

In this case, the acoustic signals were acquired at the inception voltages for PD in new oil and PD in air. The recognition rates obtained for the different features are shown in Table 14.

Table 14: Classification rates for PD in new oil and air PD

Features	Recognition Rate (%)
Sub-band Variances	100%
Sub-band Entropies	98%
Kurtosis and Skewness	88%
FFT	95%

Similar to the previous case, high recognition rates were obtained for the different types of features. Using the sub-band variances has produced a classification rate of 100. Compared to the PD signal in new oil, the corona discharge signal was almost continuous and the acoustic signals were less attenuated. This resulted in higher variance values for the wavelet sub-bands for the case corona discharge. The lowest recognition rate was produced using the skewness and kurtosis measures (88%). The histograms of PD in new oil and corona discharge are shown in Figure 42.

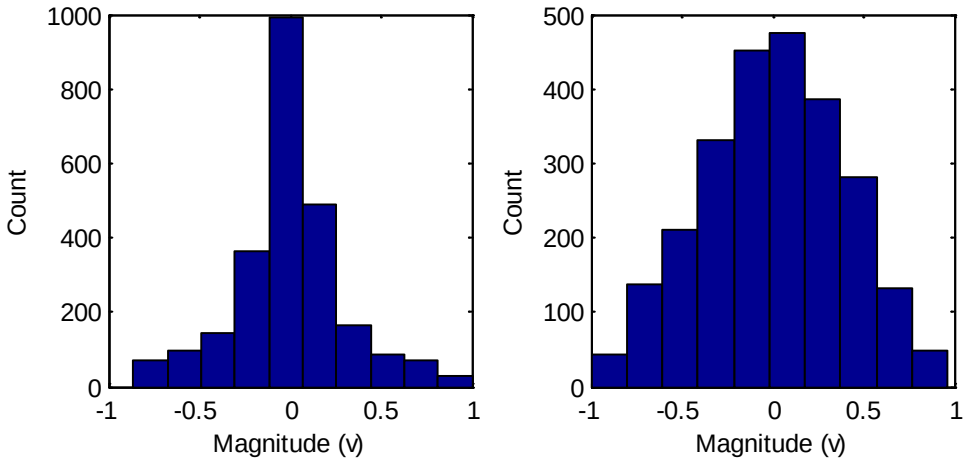

(a) (b)

Figure 42: Histogram for (a) new oil PD (b) Corona discharge signal

Based on the two histograms, the distribution of PD signal in new oil has more sharpness relative to the distribution of corona discharge. Thus, the kurtosis value is higher for PD signal in new oil. On the other hand, the two distributions are almost symmetric around the mean vale which could have reduced the recognition rate in this case.

3.4. Limitations of this work

There are some limitations that have to be considered in this research. One limitation is regarding the case where the sensor location was changed with respect to the PD source (position b). There was significant drop in the output recognition rates which indicates that the acoustic signal was highly attenuated due to the increase in the propagation distance. Thus, by considering the addition of more acoustic sensors for PD detection, the detection performance could be improved because some sensors might be closer to the PD source which leads to less attenuation for the acoustic PD signals.

Another limitation is where a larger tank size was used in PD generation. In this case also, poor recognition rates were obtained. The detected PD was highly attenuated because PD acoustic energy was scattered over a large area and there were less reflections due to the PD signals. The use of more acoustic sensors may also enhance the performance of the detection system.

4. CONCLUSIONS AND RECOMMENDATIONS

On-line monitoring of partial discharge activity is a very powerful tool for insulation diagnosis. Compared to other techniques, the acoustic detection method has several strengths. The acoustic detection is cost effective and is less susceptible for noise and electromagnetic interference. Also, multiple acoustic sensors can be employed to precisely locate the partial discharge source. The main drawback when using acoustic detection is its low sensitivity. The fact that acoustic waves suffer from high attenuation until, mandates the use of artificial intelligence tools to enhance the detection reliability.

In this research, an artificial neural network was utilized to enhance the acoustic detection of PD signals under different conditions. Those conditions include the presence of some barriers in the propagation path of the acoustic signals like paper insulation and transformer core material. The different types of features produced high recognition rates which reflects a strong correlation between the features extracted and the ability to detect acoustic PD signals. Also, the status of transformer insulation was evaluated based on the detected PD signals. The comparison was conducted between acoustic partial discharge signals acquired in new oil and aged oil. High recognition rates were obtained using the different types of features. Classification of PD activity that occurred within the oil tank and corona discharge was also performed. It was found that high classification rates can be obtained when comparing the air PD to PD in new or old oil. In addition, the effect of long propagation distances on the detection of acoustic PD signal was considered. The PD source was located in different point and some selected features were extracted from the acoustic signals with and without PD. It was verified that using features like the sub-band entropies and the FFT coefficients would enhance the detection performance. Also, the effect of insulation aging on the identification of PD signals was studied. Compared to the case of new oil, recognition rates dropped significantly except for the sub-band entropies. The recognition rates obtained using the sub-band entropies was around 90% which shows that it has good discriminating ability. In order to verify the generalization capability of the trained neural network, the training was done with acoustic signals acquired in a small tank while testing was performed using signals acquired in a larger tank size. Poor recognition rates were obtained for the different types of features in this case. Then, signals acquired in the

big tank were used for training and testing the neural network. There was significant improvement in the recognition rates when using the sub-band entropy measure.

It can be concluded that the reliability of acoustic PD detection under different conditions can be enhanced through utilizing artificial neural networks. The selection of features is important and it can highly influence the detection performance. Also, through all the experiment, the sub-band entropy measure has produced high recognition rates. The skewness and kurtosis measures showed a high sensitivity for the magnitude of the PD signal which indicates that they are not reliable features for detecting highly attenuated PD signals. On the other hand, it was verified that the use of an acoustic sensor in the low frequency range (20-80 kHz) can provide good detection performance. The high classification rates obtained when comparing acoustic PD signals in new oil and old oil shows that utilizing acoustic PD detection with the aid of artificial neural network can provide very good tool for insulation diagnosis.

For future work, it is recommended to use external triggering circuit for acoustic PD detection. It was found that due the high time resolution required for acquiring the RF signal, only few acoustic PD signals were captured. By acquiring a longer time domain signal, more acoustic PD events can be captured acoustic signal which might enhance the neural network performance. It is also recommended to use a transformer model that would better simulate the actual case. When using different tank size, comprehensive data for several tank sizes is required for training the neural network. Thus the neural network can perform the classification between the different tank sizes at the first stage and then it can match the recognized tank size with the corresponding feature vector. Finally, different types of classifiers types can be used.

5. REFERENCES

[1] A. Akbari, et al., "Transfer Function-Based Partial Discharge Localization in Power Transformers: A Feasibility Study," *IEEE Electrical Insulation Magazine*, Vol. 18, No. 5, September/October 2002.

[2] A. Kelen, " Trends in PD Diagnostics When New Options Proliferat, So Do Old and New Problems," *IEEE Transactions on Dielectrics and Electrical Insulation*, vol. 2, No.4, pp. 598-606, August 2001.

[3] T. Boczar, "" Identification of a Specific Type of PD from Acoustic Emission Frequency Spectra," *IEEE Transactions on Dielectrics and Electrical Insulation*, vol. 8, No. (4), pp. 529-534, 1995.

[4] E. Lemke, P. Schmiegel, "Introduction to Fundamentals of PD Diagnosis," *hvtestanddiagnostics.com*, [online], Available: http://hvtestanddiagnostics.com/images/publications/intro-us.pdf [Accessed: Feb. 10,2010].

[5] S. Boggs, " Partial Discharge: Overview and Signal Generation," *IEEE Electrical Insulation Magazine*, Vol. 6, No. 4, July/August 1990.

[6] C. Chen, et al., "Comparison and Analysis of Online Partial Discharge Detection Measurements for Gas Insulated Substation," *Asia Pacific Conference on NDT*, Nov. 2006, Auckland, New Zealand.

[7] M. Muhr, R. Schwarz, S. Pack and B. Koerbler "Unconventional Partial Discharge Measurements," *Annual Report Conference on Electrical Insulation and Dielectric Phenomena*, 2004

[8] Y. Tian, et al., "Comparison of Online Partial Discharge Detection Methods for HV Cable Joints," *IEEE Transactions on Dielectrics and Electrical Insulation*, vol. 9, No. (4), pp. 604-615, August 2002.

[9] P. Anita, P. Caesario and Suwarno, "Partial Discharge Diagnosis of Gas Insulated Station (GIS) Using Acoustic Method," *International Conference on Electrical Engineering and Informatics*, 2009, Selangor, Malaysia.

[10] C. Su, et al, "Detection of Partial Discharge in Cast-resin Dry-type Transformer by Using Acoustic Emission Technique," *16th WCNDT 2004 - World Conference on NDT*, Montreal, Canada.

[11] K. Prasanta, N. Kishore, A. Sinha, "Simulation and Analysis of Acoustic Wave Propagation due to Partial Discharge Activity," *Annual Report Conference on Electrical Insulation and Dielectric Phenomena*, 2006.

[12] Y. Tian, et al, "Application of Acoustic Emission Techniques and Artificial Neural Networks to Partial Discharge Classification," *IEEE International Symposium on Electrical Insulation*, Boston, USA, April 2002

[13] M. Abdel Salam, et al., "Partial Discharge Classification through Wavelet Packets of Their Modulated Ultrasonic Emission," *Intelligent Data Engineering and Automated Learning*, 2004.

[14] T. Boczar, S. Borucki, A. Cichon and D. Zmarzly, "Application Possibilities of Artificial Neural Networks for Recognizing Partial Discharges Measured by the Acoustic Emission Method," *IEEE Trans. on Dielectrics and Electrical Insulation*, Vol. 16, No. 1, February 2009.

[15] C. Kuo, H. Shieh, "Artificial Classification System of Aging Period Based on Insulation Status of Transformers," *Eighth International conference on machine learning and cybernetics*, Baoding, July 2009.

[16] J. Foo, P. Ghosh, "Artificial Neural Network Modelling of Partial Discharge Parameters for Transformer Oil Diagnosis," *Annual Conference of Electrical Insulation and Dielectric Phenomena*, 2002.

[17] S. Sovilj, R. Magjarevic and G. Rajsman, "Classification Methods for Atrial Fibrillation Prediction after CABG," *11th Mediterranean Conference on Medical and Biomedical Engineering and Computing 2007*, Ljubljana, Slovenia.

[18] R. Coifman and M. Wickerhauser, "Entropy-Based Algorithms for Best Basis Selection," *IEEE Trans. on Information Theory*, Vol. 38, No. 2, pp. 713-718, March 1992.

[19] University of Huston, "Measurments of Health and Excersize Science," *University of Huston* [Online]. Available:http://grants.hhp.coe.uh.edu/doconnor/PEP6305/Topic%20002%20Organizing%20Data2.3.htm. [Accessed: Mar. 20, 2010].

APPENDIX A MATLAB CODE

```
Plotting frequency and time domain signals:

% filename=['C:\Documents and Settings\User\Desktop\4-2-
2010\data_9_1_voltage level_metallic barrier\@2.8\AS25_3.xls'];
% filename=['C:\Documents and
Settings\User\Desktop\readings_2_1_2010\@2.4\AS2_2.xls'];
t= 0:2e-7:5e-4-2e-7;
fs=5000000;
% x=NPN(64,:);
n = 4; Wn = [25000  75000]/fs*2;
        [b,a] = butter(n,Wn);
% signal=x;
signal=OPN(32,:);
signal1=AOP(65,:);
f_sig=filter(b,a,signal);
f_sig1=filter(b,a,signal1);
f=(1/(t(1,9)-t(1,8)))*(-1*(length(f_sig)/2):(length(f_sig)/2)-
1)/length(f_sig);
L=length(signal);
spec=abs(fftshift(fft(f_sig)))/L;
spec2=abs(fftshift(fft(f_sig1)))/L; %   compute FFT coefficients
%
figure(1)
subplot(1,2,1),plot(f,spec)
title ('(a)')
xlim([0,80000])
xlabel('Frequency (Hz)'),ylabel('Magnitude (v)')
subplot(1,2,2),plot(f,spec2)
xlim([0,80000])
title ('(b)')
xlabel('Frequency (Hz)'),ylabel('Magnitude (v)')

[c,l] = wavedec(f_sig,5,'db15'); %   WT decomposition
[c1,l] = wavedec(f_sig1,5,'db15');
        a5=c(1:l(1));
        d5=c(l(1)+1:2*l(1));
        d4=c(2*l(1)+1:2*l(1)+l(3));
        d3=c(2*l(1)+l(3)+1:2*l(1)+l(3)+l(4));
        d2=c(2*l(1)+l(3)+l(4)+1:2*l(1)+l(3)+l(4)+l(5));
        d1=c(2*l(1)+l(3)+l(4)+l(5)+1:2*l(1)+l(3)+l(4)+l(5)+l(6));

        a51=c1(1:l(1));
        d51=c1(l(1)+1:2*l(1));
        d41=c1(2*l(1)+1:2*l(1)+l(3));
        d31=c1(2*l(1)+l(3)+1:2*l(1)+l(3)+l(4));
        d21=c1(2*l(1)+l(3)+l(4)+1:2*l(1)+l(3)+l(4)+l(5));
        d11=c1(2*l(1)+l(3)+l(4)+l(5)+1:2*l(1)+l(3)+l(4)+l(5)+l(6));

% Plotting commands
%figure(3)
%
%     xlim([0,5e-4-2e-7]);
%
%     subplot(5,2,1),plot(t,OPN(32,:)),title('(a)')
%
```

```
%     subplot(5,2,3),plot(d3),title(['d',num2str(3)]);
%
%     subplot(5,2,5),plot(d4),title(['d',num2str(4)]);
%
%     subplot(5,2,7),plot(d5),title(['d',num2str(5)]);
%
%     subplot(5,2,9),plot(a5),title(['a',num2str(5)]);
%
%
%
%     subplot(5,2,2),plot(t,AOP(64,:)),title('(b)')
%     xlim([0,5e-4-2e-7]);
%
%     subplot(5,2,4),plot(d31),title(['d',num2str(3)]);
%
%     subplot(5,2,6),plot(d41),title(['d',num2str(4)]);
%
%     subplot(5,2,8),plot(d51),title(['d',num2str(5)]);
%
%     subplot(5,2,10),plot(a51),title(['a',num2str(5)]);



%     xlabel('Time (s)')

% figure(4)
% subplot(1,2,1),hist(f_sig)
% title('Histogram of acoustic PD signal')
% xlabel('Magnitude (v)'),ylabel('Frequency')
% subplot(1,2,2),hist(f_sig1)
% title('Histogram of acoustic signal with no PD')
% xlabel('Magnitude (v)'),ylabel('Frequency')
%     subplot(3,2,1),plot(D1),title(['D',num2str(1)]);
%     subplot(3,2,2),plot(D2),title(['D',num2str(2)]);
%     subplot(3,2,3),plot(D3),title(['D',num2str(3)]);
%     subplot(3,2,4),plot(D4),title(['D',num2str(4)]);
%     subplot(3,2,5),plot(D5),title(['D',num2str(5)]);
%     xlabel('Time (s)'),ylabel('Magnitude')
%%%%%%%%%%%%%%NN%%%%%%%%%%%%%%%
%%%%%%%%%%%%%%%%%%%%%%%%%%%%%%%%%%%%%
close all;
clear all;
clc;
 fs=5000000;
load NPN
load BHPN
%%
%%%%%%%%%%%%%%Training%%%%%%%%%%%%%%%
%%%%%%%%%%%%%%%%%%%%%%%%%%%%%%%%%%%%%
Train_set = []; % Initiate training vector
Test_set=[]; % Initiate testing vector
% load BHPN;

n = 4; Wn = [25000  75000]/fs*2; % Band-pass Butterworth Filter

        [b,a] = butter(n,Wn); % Filtering
%%
    for j=1:50;
        signal=NPN12(j,:);
```

```
        f_sig=filter(b,a,signal);
        L=length(signal);
        spec=abs(fftshift(fft(f_sig)))/L; % Evaluate FFT
coefficients
        [c,l] = wavedec(f_sig,5,'db15'); % perform WT decomposition
%         pha=angle(fftshift(fft(f_sig)))/L;
%         ATR1= appcoef(c1,l1,'db15',4);
%
%
%        subplot(2,1,1)
        a5=c(1:l(1));
        d5=c(l(1)+1:2*l(1));
        d4=c(2*l(1)+1:2*l(1)+l(3));
        d3=c(2*l(1)+l(3)+1:2*l(1)+l(3)+l(4));
        d2=c(2*l(1)+l(3)+l(4)+1:2*l(1)+l(3)+l(4)+l(5));
        d1=c(2*l(1)+l(3)+l(4)+l(5)+1:2*l(1)+l(3)+l(4)+l(5)+l(6)); %
evaluate WT coefficients
%             E_a5=wentropy(a5,'log energy');
%             E_d5=wentropy(d5,'log energy');
%             E_d4=wentropy(d4,'log energy');
%             E_d3=wentropy(d3,'log energy');
%             E_d2=wentropy(d2,'log energy');
%             E_d1=wentropy(d1,'log energy');
            E_a5=wentropy(a5,'shannon');
            E_d5=wentropy(d5,'shannon');
            E_d4=wentropy(d4,'shannon');
            E_d3=wentropy(d3,'shannon');
            E_d2=wentropy(d2,'shannon');
            E_d1=wentropy(d1,'shannon');
            ATR1=[var(a5) var(d5) var(d4) var(d3) var(d2) var(d1)];
% variance of wavelet sub-bands
%         ATR1=[kurtosis(f_sig) skewness(f_sig)];
%          ATR1=[wentropy(signal,'shannon');wentropy(signal,'log
energy')];
%          ATR1=[wentropy(signal,'shannon');kurtosis(signal)];
%          t=wentropy(signal,'shannon');
%          ATR1=[t t*t t*t*t sqrt(t)];
%         ATR1=[var(a5) var(d5) var(d4) var(d3) var(d2) var(d1)];
%             ATR1=wentropy(f_sig,'log energy');
%             ATR1=E_d1;
%             ATR1=E_d5;
%             ATR1=E_d1;
%             ATR1=wentropy(f_sig,'shannon');
%         ATR1=spec(1251:1285);
%             ATR2=ATR1';
%         for  k=1:10
%             ATR(k,:)=mean(ATR2(10*(k-1)+1:10*k,:));
%         end
        Train_set=[Train_set;ATR1];
    end
    %%

    for k=1:50;
        signal=NPN24(k,:);
%
        f_sig=filter(b,a,signal);
        L=length(signal);
%         f_sig=f_sig/max(f_sig);
        spec=abs(fftshift(fft(f_sig)))/L;
        [c,l] = wavedec(f_sig,5,'db15');
%         pha=angle(fftshift(fft(f_sig)))/L;
```

```
%
%

%         ATR1= appcoef(c1,l1,'db15',4);
%             [c1,l1] = wavedec(signal(:,1),5,'db15');
%             m= detcoef(c1,l1,'db15',3);
        a5=c(1:l(1));
        d5=c(l(1)+1:2*l(1));
        d4=c(2*l(1)+1:2*l(1)+l(3));
        d3=c(2*l(1)+l(3)+1:2*l(1)+l(3)+l(4));
        d2=c(2*l(1)+l(3)+l(4)+1:2*l(1)+l(3)+l(4)+l(5));
        d1=c(2*l(1)+l(3)+l(4)+l(5)+1:2*l(1)+l(3)+l(4)+l(5)+l(6));
%             m1=m(3);
%             ATR1= cell2mat(m1);
%          ATR1=kurtosis(f_sig);
%          ATR1=skewness(signal);
%          ATR1=wentropy(signal,'log energy');
%             E_a5=wentropy(a5,'log energy');
%             E_d5=wentropy(d5,'log energy');
%             E_d4=wentropy(d4,'log energy');
%             E_d3=wentropy(d3,'log energy');
%             E_d2=wentropy(d2,'log energy');
%             E_d1=wentropy(d1,'log energy');
            E_a5=wentropy(a5,'shannon');
            E_d5=wentropy(d5,'shannon');
            E_d4=wentropy(d4,'shannon');
            E_d3=wentropy(d3,'shannon');
            E_d2=wentropy(d2,'shannon');
            E_d1=wentropy(d1,'shannon');
%             ATR1=E_d5;
%             ATR1=E_d1;
%             ATR1=wentropy(f_sig,'log energy');
%             ATR1=[E_a5 E_d5 E_d4 E_d3 E_d2 E_d1 spec(1263:1285)];
%             ATR1=[E_a5 E_d5 E_d4 E_d3 E_d2 E_d1 var(a5) var(d5)
var(d4) var(d3) var(d2) var(d1)];
%             ATR1=[kurtosis(f_sig) skewness(f_sig) E_a5 E_d5 E_d4
E_d3 E_d2 E_d1];
%             ATR1=[kurtosis(f_sig) skewness(f_sig) var(d5) var(d4)
var(d3) var(d2) var(d1)];
%             ATR1=[kurtosis(f_sig) skewness(f_sig)];
%          ATR1=wentropy(f_sig,'shannon');
%            ATR1=[wentropy(signal,'shannon');kurtosis(signal)];
%             t=wentropy(signal,'shannon');
%             ATR1=[t t*t t*t*t sqrt(t)];
%             ATR1=spec(1251:1285);
        ATR1=[var(a5) var(d5) var(d4) var(d3) var(d2) var(d1)];
%             ATR1=E_d1;
%         ATR2=ATR1';
%         for  k=1:10
%             ATR(k,:)=mean(ATR2(10*(k-1)+1:10*k,:));
%         end
        Train_set=[Train_set;ATR1];
    end


 %%
```

```
for j=1:10;
        signal=BHPN12C(j,:);

        f_sig=filter(b,a,signal);
        L=length(signal);
%         f_sig=f_sig/max(f_sig);
        spec=abs(fftshift(fft(f_sig)))/L;
        [c,l] = wavedec(f_sig,5,'db15');
%         pha=angle(fftshift(fft(f_sig)))/L;

        a5=c(1:l(1));
        d5=c(l(1)+1:2*l(1));
        d4=c(2*l(1)+1:2*l(1)+l(3));
        d3=c(2*l(1)+l(3)+1:2*l(1)+l(3)+l(4));
        d2=c(2*l(1)+l(3)+l(4)+1:2*l(1)+l(3)+l(4)+l(5));
        d1=c(2*l(1)+l(3)+l(4)+l(5)+1:2*l(1)+l(3)+l(4)+l(5)+l(6));
%          ATS1=kurtosis(f_sig);
%          ATS1=skewness(signal);
%          ATS1=wentropy(signal,'log energy');
%         ATS1=wentropy(f_sig,'shannon');
%             ATS1=[wentropy(signal,'shannon');kurtosis(signal)];
%             t=wentropy(signal,'shannon');
%         ATS1=[kurtosis(f_sig) skewness(f_sig)];
%             E_a5=wentropy(a5,'log energy');
%             E_d5=wentropy(d5,'log energy');
%             E_d4=wentropy(d4,'log energy');
%             E_d3=wentropy(d3,'log energy');
%             E_d2=wentropy(d2,'log energy');
%             E_d1=wentropy(d1,'log energy');
            E_a5=wentropy(a5,'shannon');
            E_d5=wentropy(d5,'shannon');
            E_d4=wentropy(d4,'shannon');
            E_d3=wentropy(d3,'shannon');
            E_d2=wentropy(d2,'shannon');
            E_d1=wentropy(d1,'shannon');
            ATS1=[var(a5) var(d5) var(d4) var(d3) var(d2) var(d1)];
%             ATS1=[E_a5 E_d5 E_d4 E_d3 E_d2 E_d1 spec(1263:1285)];
%             ATS1=[E_a5 E_d5 E_d4 E_d3 E_d2 E_d1 var(a5) var(d5)
var(d4) var(d3) var(d2) var(d1)];
%             ATS1=[kurtosis(f_sig) skewness(f_sig) E_a5 E_d5 E_d4
E_d3 E_d2 E_d1];
%             ATS1=[kurtosis(f_sig) skewness(f_sig) var(d5) var(d4)
var(d3) var(d2) var(d1)];
%             ATS1=[t t*t t*t*t sqrt(t)];
%             ATS1=spec(1251:1285);
%         ATS1=E_d1;
%             ATS1=E_d5;
%             ATS1=E_d1;
%             ATS1=wentropy(f_sig,'log energy');
%         ATS2=ATS1';
%         for  k=1:10
%             ATS(k,:)=mean(ATS2(10*(k-1)+1:10*k,:));
%         end
        Test_set=[Test_set;ATS1];
end
    for k=1:10;
        signal=BHPN24C(k,:);

        f_sig=filter(b,a,signal);
        L=length(signal);
%         f_sig=f_sig/max(f_sig);
```

```
        spec=abs(fftshift(fft(f_sig)))/L;
        [c,l] = wavedec(f_sig,5,'db15');
%         pha=angle(fftshift(fft(f_sig)))/L;
%
        a5=c(1:l(1));
        d5=c(l(1)+1:2*l(1));
        d4=c(2*l(1)+1:2*l(1)+l(3));
        d3=c(2*l(1)+l(3)+1:2*l(1)+l(3)+l(4));
        d2=c(2*l(1)+l(3)+l(4)+1:2*l(1)+l(3)+l(4)+l(5));
        d1=c(2*l(1)+l(3)+l(4)+l(5)+1:2*l(1)+l(3)+l(4)+l(5)+l(6));
%          ATS1=kurtosis(f_sig);
%          ATS1=skewness(signal);
%         ATS1=[kurtosis(f_sig) skewness(f_sig)];
%          ATS1=wentropy(signal,'log energy');
%          ATS1=wentropy(f_sig,'shannon');
%             t=wentropy(signal,'shannon');
%            ATS1=[t t*t t*t*t sqrt(t)];
%             E_a5=wentropy(a5,'log energy');
%             E_d5=wentropy(d5,'log energy');
%             E_d4=wentropy(d4,'log energy');
%             E_d3=wentropy(d3,'log energy');
%             E_d2=wentropy(d2,'log energy');
%             E_d1=wentropy(d1,'log energy');
            E_a5=wentropy(a5,'shannon');
            E_d5=wentropy(d5,'shannon');
            E_d4=wentropy(d4,'shannon');
            E_d3=wentropy(d3,'shannon');
            E_d2=wentropy(d2,'shannon');
            E_d1=wentropy(d1,'shannon');
            ATS1=[var(a5) var(d5) var(d4) var(d3) var(d2) var(d1)];
%         ATS1=E_d1;
%             ATS1=[E_a5 E_d5 E_d4 E_d3 E_d2 E_d1 spec(1263:1285)];
%             ATS1=[E_a5 E_d5 E_d4 E_d3 E_d2 E_d1 var(a5) var(d5)
var(d4) var(d3) var(d2) var(d1)];
%             ATS1=[kurtosis(f_sig) skewness(f_sig) E_a5 E_d5 E_d4
E_d3 E_d2 E_d1];
%             ATS1=[kurtosis(f_sig) skewness(f_sig) var(d5) var(d4)
var(d3) var(d2) var(d1)];
%             ATS1=E_d1;
%             ATS1=wentropy(f_sig,'log energy');
%             ATS1=E_a5;
%             ATS1=spec(1251:1285);
%             ATS2=ATS1';
%         for  k=1:10
%             ATS(k,:)=mean(ATS2(10*(k-1)+1:10*k,:));
%         end
        Test_set=[Test_set;ATS1];
    end


%%
Tr = Train_set; % Training vector
Ts = Test_set; % Testing vector
Tr = abs(Tr);
Ts = abs(Ts);
TG = zeros(100,2); % initiate target matrix
for i = 1:2;
    TG(50*(i-1)+1:(i*50),i) = 1; % set the target vector
end
maxima = max([max(max(Tr)) max(max(Ts))]);
Tr = Tr/maxima;
Ts = Ts/maxima; %%%%%%%%%% Normalization
```

```
%%
%%%%%%%%%%%%%%%%%%%%%%%%%%%%%%%%%%
X= Tr;%
P=X';
net=newff(P,TG',10,{'tansig'},'trainlm');
net.performFcn = 'mse';
%%%%%%%%%%%%%%%%%%%%%%%%%%%%%% Training
%%%%%%%%%%%%%%%%%%%%%%%%%%%%%%%%%%%%%%
net.trainParam.epochs = 1000;%number of epochs
%%
net = train(net,P,TG');
%%
Y = sim(net,Ts');
for i = 1:20;
    [val ind] = sort(Y(:,i), 'descend');
    rec(i)=ind(1);
end

%%%%%%%%%%%%%%%%%%%%%%%%%%%%%%%%%%%% recognition rate %%%%%%%%%
c = 1:2;
d = repmat(c,10,1);
d = d(:)';
rec - d;
N = length(find(rec-d==0));
rate = N / 20; %
%%
%% Plotting features in 2-D space
x1=zeros(60,1);
x2=zeros(60,1);
x111=zeros(60,1);
x1=[];
x2=[];
load OPN;
x11=[OPN(1:60,:)];
x22=[OPN(61:120,:)];
 fs=5000000;
n = 4; Wn = [25000  75000]/fs*2;
        [b,a] = butter(n,Wn);


for i=1:60
    x11(i,:)=x11(i,:);
    f_sig=filter(b,a,x11(i,:));
%     f_sig=x11(i,:);
%     f_sig=f_sig./max(f_sig);
    [c,l] = wavedec(f_sig,5,'db15');
%         ATR1= appcoef(c1,l1,'db15',4);
%             [c1,l1] = wavedec(signal(:,1),5,'db15');
%
        a5=c(1:l(1));
        d5=c(l(1)+1:2*l(1));
        d4=c(2*l(1)+1:2*l(1)+l(3));
        d3=c(2*l(1)+l(3)+1:2*l(1)+l(3)+l(4));
        d2=c(2*l(1)+l(3)+l(4)+1:2*l(1)+l(3)+l(4)+l(5));
%         x1(i)=wentropy(d5,'shannon');
        x1(i)=kurtosis(f_sig);


%         x1(i)=var(d5);
end
```

```
for i=1:60
        x11(i,:)=x11(i,:);
        f_sig=filter(b,a,x11(i,:));
%         f_sig=x11(i,:);
%         f_sig=f_sig./max(f_sig);
        [c,l] = wavedec(f_sig,5,'db15');
%         ATR1= appcoef(c1,l1,'db15',4);
%             [c1,l1] = wavedec(signal(:,1),5,'db15');
%
        a5=c(1:l(1));
        d5=c(l(1)+1:2*l(1));
        d4=c(2*l(1)+1:2*l(1)+l(3));
        d3=c(2*l(1)+l(3)+1:2*l(1)+l(3)+l(4));
        d2=c(2*l(1)+l(3)+l(4)+1:2*l(1)+l(3)+l(4)+l(5));
%         x2(i)=wentropy(a5,'shannon');
        x2(i)=skewness(f_sig);


%         x2(i)=var(d5);
end
% maxima = max([max(max(x1)) max(max(x2))]);

% x2=x2/max(x2);
% x1=x1/max(x1);
% scatter(x1,aa,'r*')
%         hold on
%         bb=[7:0.1:13];
        scatter(x2,x1,'ko')
%         hold on
%         scatter(x2,x1)

% plot(x1)
% plot(x1,,x2,)
% shg
% hold on
% plot(x2,'ro')
% title('old oil PD vs no pd PD_shannon ')
% shg
% xt=[Tr(1:50,:);Tr(51:100,:)];
% xs=[Ts(1:10,:);Ts(11:20,:)];
% % xt=[x1(1:50);x2(1:50)];
% % xs=[x1(51:60);x2(51:60)];
% % help classify
% tr=[zeros(50,1);ones(50,1)];
% m=classify(xs,xt,tr);
```

VITAE

Anas Swedan was born on October 12, 1985 in Ajman, UAE. He was educated in the public schools and graduated from the Islamic Scientific Institute in 2003. He graduated from the American University of Sharjah with cum laude in 2007. His degree was a bachelor of science in electrical engineering.

Mr.Swedan started his practical life by joining ADDC, one of the utility companies in the emirate of Abu Dhabi. He was appointed as an installation engineer. Mr.Swedan started his master program in the electrical engineering at the American University of Sharjah in 2008**.**